MRes in Railway Systems Engineering and Integration
College of Engineering, School of Civil Engineering

University of Birmingham

Aerodynamic of the Trains in Tunnels

Samane Faramehr
Student ID: 1137392

September 2014
Supervisor: Dr Hassan Hemida

Dissertation submitted in partial fulfilment of the requirements for the award of MRes in Railway Systems Engineering & Integration

UNIVERSITY OF
BIRMINGHAM

University of Birmingham Research Archive

e-theses repository

This unpublished thesis/dissertation is copyright of the author and/or third parties. The intellectual property rights of the author or third parties in respect of this work are as defined by The Copyright Designs and Patents Act 1988 or as modified by any successor legislation.

Any use made of information contained in this thesis/dissertation must be in accordance with that legislation and must be properly acknowledged. Further distribution or reproduction in any format is prohibited without the permission of the copyright holder.

Acknowledgment

This work would not have been possible without the help of many people and organizations. First of all, I would like to thank my supervisor, Dr Hassan Hemida for his valuable guidance, support and ideas throughout this year. Dr Hemida taught me turbulent flow and computational fluid dynamics and I am very grateful for his time and effort. Secondly, I would like to thank the Birmingham Centre for Rail Research and Education, specifically Prof Chris Baker, Prof Felix Schmid and Mrs Joy Gray for creating a nice, friendly academic environment while I conducted the work of this thesis. Thanks are due to the School of Civil Engineering, University of Birmingham for granting me a scholarship for doing the MRes study.

Finally, I would like to acknowledge the computational resources and the Ansys-CFX software licences provided by the Birmingham Environment for Academic Research BEAR.

Executive summary

When a train moves through air, it generates a turbulent flow around it called a slipstream. The slipstream is associated with high air velocities and rapidly-changing pressure fields. These aerodynamic issues are still valid when a train passes a tunnel and in addition to these, the compressibility of the air around high-speed trains produces what are called “micro-pressure waves” as a result of running in a confined space. The air velocity, pressure variation and direction of the flow inside tunnels is different to the slipstream in open air. These differences depend on the size of the tunnel (cross section and length of the tunnel) and the shape and speed of the train.

In the present thesis, the effect of tunnel length on the flow and pressure inside is investigated. The investigation uses computational fluid dynamics techniques (CFD), in which a $1/25^{th}$ model of the ICE2 train is used. Two tunnel lengths are investigated; one is double the length of the other. The sliding technique is employed to simulate the movement of the train in the tunnel. The simulation uses unsteady RANS and applies the Shear Stress Transport (SST) turbulence model. The effect of tunnel length on both pressure and velocity fields is discussed. The variation of the pressure at the entrance and exit of the tunnel is also analysed and conclusions are drawn.

Table of contents

Contents

List of Figures

List of Tables

Chapter 1. Introduction

1.1 Background

Traditionally, train aerodynamic problems were not considered a priority except for drag reduction. However, with the introduction of the high-speed trains, aerodynamic effects became a major issue for both train operators and train manufacturers. When a train moves in open-air, it generates region of highly turbulent flow known as a slipstream. The slipstream is generally associated with high air velocities and rapidly-changing pressure fields. These two effects can create significant problems for passengers on platforms, trackside workers and also for the stability of high-speed trains if running in strong side winds. However, when a train passes a confined space such as a tunnel, additional aerodynamic issues appear, which are different than those in the open air. This can be explained through the underlying phenomena such as the compressibility of the air around high-speed trains due to running in a confined space, which produces pressure transients along the tunnel.

Velocity, pressure variation and direction of the flow inside tunnels are different than those around a train in open air. These differences can be related to the cross section and the length of the tunnel. Therefore, the focus of this thesis is to investigate the effect of the length of a tunnel on the pressure variation and the velocity around a high-speed train in a single-track tunnel.

1.2 Aims and Objectives

The main aim of this research project is to investigate the effect of a tunnel length on the velocity and pressure around a high-speed train. In order to fulfill this aim the following objectives were set:

1. carry out a critical literature review of the flow around trains in tunnels,
2. gain an appreciation of the different methods of investigating the flow around trains in tunnels with a specific emphasis on computational techniques,

3. create a generic train model for use in the numerical simulations and validate the numerical model with the results from the literature,
4. create a train model similar to the one used in Gilbert et al., (2013) and perform a numerical simulation around the train in a short tunnel length to obtain the flow and pressure fields,
5. repeat the numerical simulations in Objective 3 with a double tunnel length, and
6. compare the results (velocity and pressure fields) obtained from the simulation with short and long tunnels and thus investigate the effect of tunnel length.

1.3 Methodology

The present work used Computational Fluid Dynamics (CFD) simulations in order to investigate the effect of tunnel length on the pressure and velocity fields around a train. All the simulations were conducted using the commercial CFD package, Ansys CFX. To properly recreate the movement of a train through a tunnel, a sliding mesh was used. A stationary domain was used for the tunnel and surroundings and a moving domain was used for the train. To simulate the air flow around trains in tunnels, the Unsteady Reynolds Averaged Navier-Stokes (URANS) method was used. The information between the stationary and moving domains was transferred through an interface between the stationary and non-stationary domains. Details of the methodology will be presented in Chapter 3.

1.4 Structure of the report

This report presents a background of the investigated topic, followed by an introduction of the aim and objectives of the investigation. In chapter 2, a critical literature review is carried out with a focus on the aerodynamics of trains in tunnels. In Chapter 3, the methodology of the investigation is explained. The train model and tunnel dimensions are shown in chapter 4. Chapter 5 shows the mesh and numerical details of CFD simulations. The results of the simulations are analyzed in Chapter 6. Furthermore, the results are discussed in Chapter 7. Eventually, the findings are concluded in Chapter 8.

Chapter 2. Literature review

Flow around high speed trains has received considerable attention from researchers in the last three decades. Investigations have been performed using different experimental and computational techniques, including full-scale, physical modelling and numerical simulations. In what follows, a brief review of the literature regarding each method will be presented.

2.1 Full-scale measurements

There are a range of full-scale studies in train aerodynamics, investigating the aerodynamic drag of trains, cross winds, slipstream velocities and pressure transients (Baker, 2001, Baker et al, 2008, Baker, 2010a, Baker et al, 2013a, Baker et al, 2013b, and Quinn et al, 2010). Also a number of standards and codes of practice have been established for the aerodynamics of trains in open spaces (CEN, 2003, CEN, 2009, CEN, 2010). The specifications of these codes are normally based on full-scale measurements, which are a source of reliable data.

Baker et al., (2013a) studied the nature of train slipstreams using full-scale experiments. The data were presented in the form of averaged dimensionless slipstream velocities along the train length for a range of train types. The study aimed at preparing a database for TSI (Technical Specifications for Interoperability), which sets out requirements for interoperability in Europe (RSSB, 2014). Ultrasonic anemometers set at different locations were used to measure slipstream velocities for 18 different train types with different length and operational speed. The results showed that at some distance ahead of the train nose, the velocity magnitudes showed a sharp rise and reached a large peak around the train nose. This peak drops very rapidly after the nose region (the flow region close to the nose) of the train. After the nose region, an increase in slipstream velocity continues into the near wake region (up to 100 m behind the trains). The velocity magnitudes usually reach peaks between 50m and 100m behind the train tail and then reduce gradually. The results showed also that the slipstream velocity magnitude

decreases with height from the ground. It was also shown that trains with more-rounded nose or tails cause greater increases in the slipstream velocity in comparison to the less-rounded designs. Additionally, double unit trains produce large slipstream peaks at the junction of the two sets and also in the near wake region. The study provides a three-dimensional understanding of slipstreams around different trains. The effect of crosswinds on train slipstream was also discussed. It was shown that sharp noses generate thinner boundary layer along the train sides and also a steep rise of slipstream velocity in near wake region. However, when the train nose shape is relatively more rounded, faster boundary layer growth is observed while less vigorous flow occurs near wake region.

Aerodynamic phenomena in confined spaces such as tunnels have also received the attention of researchers, especially with issues of aerodynamic noise, vibration and pressure variations of high-speed trains in tunnels.

Studying the pressure variation inside tunnels is also important because, in addition to passenger discomfort issues, the pressure difference between outside and interior of the vehicles can load the components of vehicle body (CEN, 2003). Also the radiation of pressure waves at tunnel exit which generates sonic boom, which is greater for slab track rather than for ballasted track. Pressure fluctuations cause inconvenience for passengers, workers and people living or passing close to the tunnel ends, especially when the duration of these fluctuations are short and the amplitude of pressure changes is high (Reiterer et al, 2002).

Three main aerodynamic phenomena occur when a train enters a tunnel; the first is the generation of the pressure waves inside the tunnel, the second is the propagation of these waves along the tunnel length and the third is the reflection of the waves back along the tunnel length with micro pressure waves also escaping from the tunnel exit (Krylov, 2001). The pressure transients caused by trains passing through tunnels are significantly larger than those in the open air and can cause passenger discomfort, especially in poorly-sealed trains.

The first attempt to investigate the aerodynamic issues in tunnels was carried in central Japan on the Shinkansen high-speed railway. Later investigations were conducted in Europe. In the UK, the situation was more complicated due to the existing narrow Victorian tunnels having smaller loading gauges (Baker, 2010b).

Chen et al., (2012) studied the nature of pressure waves inside tunnels by means of full-scale experiment on the Taiwan high-speed line. Several operating speeds with a maximum of 300 km/h were considered for obtaining pressure time histories. These histories were measured by positioning pressure sensors at different locations in a 7 km long tunnel using tunnel hood portals. The results showed that the entry and exit of the nose of the train cause a significant positive pressure which propagates along the tunnel while the entry and exit of the tail cause negative pressures. The results showed that the wave propagates within the tunnel at nearly the speed of sound. The study also showed that, in such a long tunnel, the peak pressure remains constant during the passing of a train in locations far enough from the exit (around 50 m for this tunnel portal). It was hypothesised that the positive peak pressure inside the tunnel is related to the square of operating speed, which is in agreement with the theoretical models. However, it has been found that relating pressure troughs to train speed is not as straightforward as relating the pressure peaks. Although there are different parameters that can affect the pressure inside the tunnel such as train length, train nose and under-body blockage, these have not been included in their experimental study. In addition, although the tunnel included a high numbers of shafts along its length, there was no clear interpretation of their effects on pressure waves.

Suzuki et al., (2008) studied the aerodynamic forces on a Shinkansen train passing through a tunnel. The train experienced lateral vibrations noticeably greater than those in open air. The main aim of the study was to clarify the mechanism of the unknown aerodynamic forces around the train in the Shinkansen high-speed line and their effect on the lateral vibrations generated during operation. Four pressure gauges were installed on each side of a 16-car set Shinkansen train. Also a number of accelerometers were installed in order to measure the lateral acceleration on the car bodies. The train operating speed was 267 km/h and the tunnel was more than 2000 m in length. The results showed that when the nose of the train entered the tunnel, a compression wave was generated which was followed by an expansion wave generated inside the tunnel when the tail entered the tunnel. These pressure waves propagated ahead of the train at the speed of sound and reflected back at the tunnel exit. The waves continued travelling and reflecting

between the two portals (entrance and exit) although a portion of the compression wave radiated as a pulse from the tunnel in the form of micro pressure waves (Figure 1).

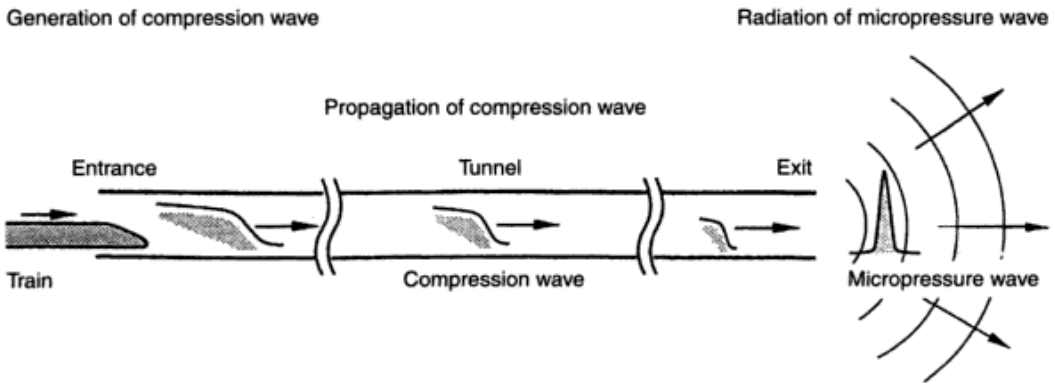

Figure 1. Generation, propagation and radiation of pressure waves (source: Krylov, 2001)

The study also found that the root mean square of the pressure fluctuation develops along the length of the first 8 cars and stabilises about a constant value along the remaining length of the train. Suzuki et al., (2008) concluded that the lateral vibration of the Shinkansen train running through tunnels originates from the development of the pressure fluctuation along the first 8 cars of the train between the train sides and the tunnel wall.

The behaviour of compression and expansion waves and their reflections are documented in CEN (2003). Figure 2 (a) demonstrates the two major wave propagations through the tunnel, from the entrance to the exit. These two main waves are caused by the entry of nose and tail of the train while the other observed minor waves are due to the reflection of the main waves (CEN, 2003). Figure 2(b) and Figure 2 (c) show the magnitude of pressure pulses seen by an observer on a train and in the tunnel, respectively. The superposition of the waves with the same signs increases the magnitude of the pressure pulses, whereas the superposition of two waves of different signs decreases the magnitude of the pressure pulses. The passing of train nose generates a localised pressure peak at a given location in the tunnel while the passing of the train tail causes a drop in the localised pressure.

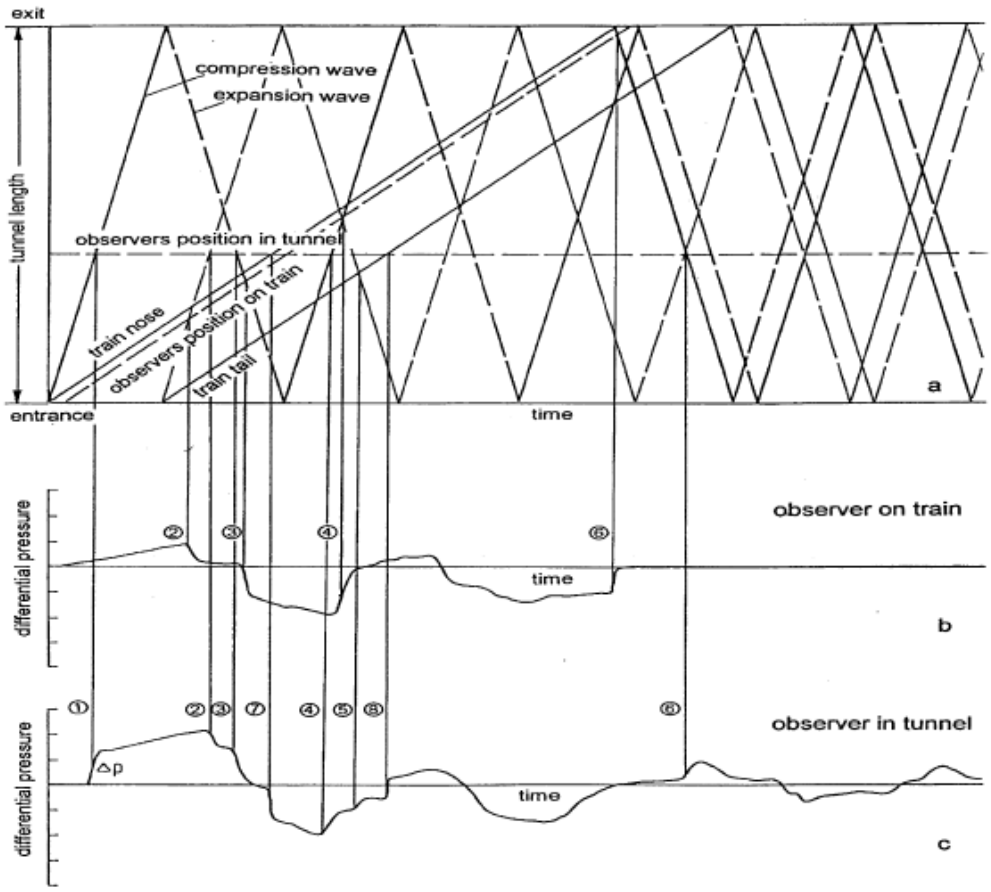

Figure 2. wave diagram and pressure transients due to a train passage through a tunnel (key: 1: initial head wave, 2: initial tail wave, 3 & 4: reflection head wave, 5: reflection tail wave, 6: exit wave, 7: passing of head, 8: passing of tail)

2.2 Physical modelling

Using full-scale experiments to investigate the velocity and pressure generated by high-speed trains in confined spaces such as tunnels is very difficult and expensive. It is more practical and economical for researchers to carry out model-scale experiments due to the more controlled environment and the possibility of investigating different parameters in a short time.

The physical modeling, in forms of moving and rotating models, has been used to study a range of aerodynamic investigations in open space problems (Baker et al., 2001, Baker et al., 2008, Baker et al., 2012a, Baker et al., 2012b, Baker et al., 2013a, Baker et al., 2013b, Gil et al., 2008, Jonsson et al., 2009, Sterling et al., 2008). So far only a few model-scale studies have been carried out for the trains passing through tunnels and other confined

spaces (over-bridges and structures). For instance, Baker et al., (2012a) investigated transient aerodynamic loads for a range of different structures in the vicinity of railway tracks using reduced-scale models. The ultimate goal of the study was to use the data to develop relevant European codes and standards, which are not specifically for UK-specific loading gauges.

It is well known that when a train passes, especially at a high speed, the generated transient pressures and forces will load the trackside structures. This transient loading affects the design of the structures located over or next to the track. The effect of a wide range of combinations of train types and the infrastructures has been investigated on aerodynamic transient loading in the laboratory test by $1/25^{th}$ scale moving model facility with operating speed of 40 m/s. The results clearly showed that in general the bluffer the train, the higher the pressure coefficient that was generated. The pressure reached the positive and negative peaks when the nose and tails of the trains approached the structures and passed the structures, respectively. When the nose of the train has passed the measurement positions, the values of the pressure were oscillating around zero (ambient pressure). More precisely, the results showed that for a hoarding structure, the negative peaks (suction imposed on the structure) are less clearly observed.

As the height of over-bridge structure increases, the magnitude of pressure coefficient reduces. In case of a canopy structure, the blunt nose train types caused vertical pressure fluctuation waves to appear in the space between canopy and platform. Trestle platform results showed that the pressure coefficient magnitudes decrease as the distance from the platform edge increases. The study correlated the pressure coefficient to slipstream velocities in broadly valid arguments. The authors also attempted to parameterize the available pressure distribution data to any structure case. Although some theoretical expressions are introduced as a useful framework for analysis and discussions, a general parameterization of data was not possible. It is concluded that the moving model methodology can be an economical method of data collection due to the validity of the results obtained in a wide range of experiments. The study not only provided a database for a wide range of available trackside structures but also attempted a quite successful theoretical correlation for future use.

Hein and Ehrenfried, (2013), investigated the phenomenon of pressure waves at the exit of a tunnel. The moving-model experiment facility based in Gottingen, Germany was used to investigate the passing of an ICE3 through a 2 m tunnel at $1/25^{th}$ scale. The operating speed of the train was between 38 m/s and 44 m/s. The blockage ratio of the model (ratio of train cross section to the tunnel cross section) was equal to 0.23, which is the case for German double-deck train passing a single rail tunnel. The results showed that when the train entered the tunnel the pressure initially increased from zero pressure (ambient pressure) to a peak at a location close to the tunnel entrance. At the same time, at a location clos to the tunnel exit pressure increased significantly less steeply. Very rapidly after the train entry, the positive pressure value reached its maximum near the entrance. This is followed by a very steep decrease in positive pressure magnitudes. The expansion wave (negative pressure) later develops due to the entry of the train tail into the tunnel. Reflections along the tunnel caused complicated forms of pressure changes at different locations of the tunnels. The behavior of the pressure waves is very similar to that of previously mentioned above. Although quite a simple pressure pattern was observed near the tunnel entrance, more complicated pressure forms including different pressure peaks with larger magnitudes have been observed in locations [further from] the entrance. This result cannot be expected by theoretical methods and the authors hypothesized that the higher magnitudes of pressure in the locations [further from] the entrance might be due to the thickness of the boundary layer or the formed vortices at the entrance.

It is important to note that the pressure gradient caused by passing trains in some cases is the most critical parameter for high-speed operation. When the pressure changes are rapid the consequences for adjacent structures or passengers can be severe. It also should be noted that the sonic boom effect is primarily influenced by pressure gradient (Vardy, 2008) and hence the pressure gradient is a crucial parameter in sonic boom studies. The entrance of a train into a small cross-section tunnel normally results in a rapid pressure change. Therefore, Hein and Ehrenfried (2013) suggested that if the duration of this pressure change increases, the pressure gradient decreases. This can be achieved by use of an extended portal with vents at the entrance.

In this case, the entire pushed flow region at the front of the train will not directly enter the tunnel but also some pressure rise has been already experienced while train passes through portals. Although in general the pressure peaks will remain the same the new design will increase the time by which this pressure change experiences. It has been concluded that this extension at the portal significantly affects the pressure gradient magnitudes. It has been suggested that the nature of the vortices in tunnels can be investigated by using smoke visualization.

The experimental investigation as a model-scale experiment lacked validation against full-scale data. The studied data are limited to demonstrate the ability of moving-models to obtain adequate pressure transient results. On the other hand, the study has not considered the effect of length of the train, length of the tunnel and portal design on the pressure in the tunnel.

Hwang et al., (2000) studied the effects of a number of parameters including train speed, blockage ratio, nose shape and air shafts on the compression wave generated by a high-speed train in a tunnel using model-scale experiments. The study intended to investigate the countermeasures to reduce the micro pressure wave effects from high-speed trains passing through tunnels. A wide range of parameters were investigated including: different nose shapes, slanted and non-slanted tunnel entries, different tunnel length, different tunnel width and different blockage ratios. The experiment was carried out for an operating speed of 83.3 m/s.

The pressure time history results have been presented in the similar way as the investigation of Hein and Ehrenfried (2013). In broad terms the pressure patterns of both studies at different locations in the tunnels were similar. The investigation showed that micro pressure wave magnitudes increase with increasing train speed. Hwang et al., (2000), showed that having a slanted entrance for a tunnel rather than a straight one helped to reduce the micro pressure wave effects at speed of around 300 km/h. The effect was to the contrary for velocities around 380 km/h. The results also showed that in case of higher blockage ratio and blunter nose shapes caused larger micro pressure waves to be generated. Airshafts have been found to be useful countermeasures to reduce pressure fluctuations and corresponding micro pressure waves.

The model geometries used in Hwang et al, (2000) were idealized and are not entirely representative of the real trains. This might have affected the results and therefore the effect of shape of the rolling stock and train with the same blockage ratio requires further investigation. To conclude, the study provided a useful database for a wide range of rolling stock and structural parameters.

Gilbert et al., (2013) studied the pressure and velocity variations in the tunnels of different lengths. Cobra probes were used to measure the velocity at different locations inside the tunnels. The probes were fixed in space and thus measure the slipstream and wake flow as would be experienced by a static observer. However, it is well known that the Cobra probes are not capable of measuring reversed flow and thus a detailed description of the flow cannot be achieved.

2.3 Numerical modelling

As previously mentioned, full-scale experiments are often expensive and time-consuming to conduct. A potential solution to overcome this problem is to use model-scale experiments. However, there are limitations when conducting physical modelling such as the amount of data that can be obtained is limited by the measurement equipment and campaign length.

Alternatively, train aerodynamics investigations can be conducted using numerical techniques in which both the flow and pressure fields can be obtained for both full- and model-scales. Numerical simulations have been used extensively to study the flow around trains subjected to crosswinds (Baker et al., 2011, Cheli et al., 2010, Hemida and Baker, 2010, Hemida and Krajnovic, 2009), slipstream investigations (Hemida et al., 2010, Hemida and Baker 2012, Huang et al, 2014, Flynn et al., 2014) and drag reduction tests (Vladimir et al., 2012 and Hong-qi, 2009). However, due to the complexities associated with the moving train simulations in CFD, few researches have been carried out to study the flow around trains in tunnels.

Baron et al, (2007) studied the nature of pressure waves induced by a high-speed train travelling through a tunnel. The study used two different methods: model–scale physical experiments and numerical simulations. The data obtained were compared in order to validate the results from both methods. The research aimed at gaining a clear

understanding of flow inside tunnels and the effect of implementing airshafts along the tunnel surface. The results showed the effect of train cross-section, length and tunnel airshafts on the compression wave produced by the train. In general, the results showed that the pressure peaks are highly dependent on the operating speed and the nose shape. The study also investigated the effect of different cross-sectional shapes of trains on the pressure magnitudes while keeping the nose shape and blockage ratio constant. The methodologies were robust enough to show the pressure reduction due to introduction of the shafts to the tunnels. A good agreement was observed between the numerical and experimental results however the data failed to show the periodic fluctuations observed in the full-scale experiments after the initial pressure growth and peaks. This is hypothesised to be due to the limited wave dissipation in laboratory experiment compared to full scale.

Khayrullina et al., (2014), studied the flow around Dutch passenger and freight trains running through underground tunnels using transient CFD simulations. The research considered factors influencing the strength of pressure waves inside a tunnel such as blockage ratio, train speed, portal shape, tunnel length and roughness. The study found that the passenger train caused higher velocities than the freight train because of a higher operating speed and lower blockage ratio. A slipstream velocity exceeding 5 m/s was considered a discomfort wind speed, while, any slipstream velocity exceeding 12 m/s as a dangerous wind speed. Hence, the investigation of the velocity in the tunnel showed that exceeding the discomfort threshold normally occurs at distances between 1.2 m to 2.9 m from the platform edge in the case of the passenger train. It has been found that dangerous wind gusts do not occur for a freight train passing at 100 km/h. The study mainly focused on the investigating the danger and discomfort zones in Dutch underground stations and lacks a comprehensive visualization of the flow.

Hwang et al, (2000) attempted to visualise the propagation of compression waves through a tunnel using CFD. The visualisation showed that the compression wave formed inside the tunnel before the train entered the tunnel and also the compression wave propagated through tunnel exit faster than the train itself. The speed of this propagation was shown to be equal to the sound speed with agreement to other work in the literature.

CFD method also performed well in investigating the micro pressure waves. Liu et al., (2013), investigated the aerodynamic behaviour of a freight train passed by an ICE2 passenger train using Large Eddy Simulation. Regarding the confinement that the trains caused for on another the aerodynamic loads on both train types were obtained. The results showed that the reduction in track spacing of two trains increased the aerodynamic forces on both trains passing each other.

From the available literature and to the best of the author's knowledge, the effect of the tunnel length on both the flow and pressure fields around the train and inside the tunnel has not been properly investigated. Thus the main aim of the present thesis is to study a moving train model in a single-track tunnel using numerical simulations.

2.4 Analytical methods

Although computational and experimental tools offer detailed ways of investigations for train aerodynamics, in some circumstances straightforward analytical methodologies are adequate. Especially in cases of investigating pressure transients in tunnels one-dimensional analyses are quite sufficient for practical issues (Baker, 2014). There are a number of studies investigating the train aerodynamic in tunnels mainly by using one-dimensional analytical methods (Howe, 2003a, Howe, 2003b and Vardy, 2008). For instance, Howe et al., (2000), studied the compression waves generated by a high-speed train passing a tunnel theoretically. The study showed that the pressure rise across the wave is directly proportional to mean air density, train speed and the cross sectional area of the train. Furthermore, Howe et al., (2003), studied a theoretical prediction of compression waves for a train passing a tunnel with unvented entrance hood. Some experiments have also been conducted and the theoretical predictions are found to be in an excellent agreement with the experimental data.

Chapter 3. Methodology

There are different ways to obtain the velocities and pressures around a moving body. These include full-scale measurements, physical modeling, analytical solutions and computational fluid dynamics. The analytical solution is possible only for very simplified two dimensional laminar cases, which are not of engineering interest. For many cases the full-scale measurements are difficult and/or expensive to perform. Although physical modelling is feasible for many engineering cases it also suffers from many drawbacks which include scaling problems and measurement constraints. For instance, measuring the entire three-dimensional velocity field around a moving body is impossible because data can only be obtained from a limited number of points due to time-constraints. The alternative is to use the computational fluid techniques, in which the full three-dimensional velocity and pressure field can be obtained in an affordable way.

3.1 Computational fluid dynamics

Fluid flow around moving bodies is normally turbulent, in which case the velocity and pressure fields are fluctuating in both time and space. There is no analytical solution for the governing equations of turbulent flows, instead one needs to simplify these equations to be able to solve them numerically. Computational fluid dynamics (CFD) is a technique to solve the governing equations of the fluid flow using complex numerical algorithms.

3.2 Governing equations

The equations governing the fluid motion are called the Navier-Stokes equations. These equations are derived from first principles of conservation of mass (continuity equation), momentum and energy. These equations are shown below.

Continuity equation

This equation takes the form:

$$\frac{\partial \rho}{\partial t} + \frac{\partial (\rho u_i)}{\partial x_i} = 0, \tag{1}$$

where ρ, t, u_i are the density, time and velocity components in the i direction, respectively.

In Equation 1, the density ρ is not constant but depends on the pressure and temperature.

Momentum equations

These equations take the following tensor form:

$$\frac{\partial (\rho u_i)}{\partial t} + \frac{\partial (u_j \rho u_i)}{\partial x_j} + \frac{\partial p}{\partial x_i} - \frac{\partial \tau_{ij}}{\partial x_j} = 0 \tag{2}$$

Energy equation

The conservation of energy yields the following differential equation:

$$\frac{\partial (\rho E)}{\partial t} + \frac{\partial (u_j \rho E)}{\partial x_j} - \frac{\partial}{\partial x_i}\left(k \frac{\partial T}{\partial x_i}\right) + \frac{\partial (u_j p)}{\partial x_j} + \frac{\partial (\tau_{ij} u_j)}{\partial x_j} = 0 \tag{3}$$

Where T is the temperature, τ_{ij} is the shear stress and E is the total energy.

3.3 Reynolds Average Navier Stokes equations

In a turbulent flow, the variables fluctuate randomly in both time and space and statistical approaches can be used to describe the flow. The flow variables can be decomposed into mean and fluctuating components, which is the basis of the Reynolds decomposition, Flow variables in the present work can be expressed as:

$$u = \overline{u} + u' \tag{4}$$

$$p = \overline{p} + p' \tag{5}$$

$$T = \overline{T} + T' \tag{6}$$

In many cases it is easier to analyze the time-averaged quantities. Thus the Reynolds decomposition is applied into the governing equations to obtain what is called the Reynolds Averaged Navier Stokes (RANS) equations. These equations take the form:

$$\frac{\partial \rho}{\partial t} + \frac{\partial (\rho \overline{u}_i)}{\partial x_i} = 0, \tag{7}$$

$$\rho \frac{\partial \overline{u}_i}{\partial t} + \rho \overline{u}_j \frac{\partial \overline{u}_i}{\partial x_j} = -\frac{\partial \overline{p}}{\partial x_i} + \frac{\partial}{\partial x_j}\left(\rho v \frac{\partial \overline{u}_i}{\partial x_j} - \rho \overline{u_i' u_j'} \right), and \tag{8}$$

$$\frac{\partial \overline{T}}{\partial t} + \frac{\partial \overline{T}\,\overline{u_j}}{\partial x_j} = \frac{\partial}{\partial x_j}\left[\frac{v}{Pr} \frac{\partial \overline{T}}{\partial x_j} - \left(\overline{T u_j} - \overline{T}\,\overline{u_j} \right) \right] \tag{9}$$

for the continuity, momentum and energy equations, respectively. The last term in the momentum equations, $\rho \overline{u_i' u_j'}$ are the Reynolds stresses, which are unknown and need modelling.

The model used to approximate the Reynolds stresses in the present work was the Shear Stress Transport *k-ω* (SST *k-ω*) model—for more information about the model please see Wilcox (1994).

Chapter 4. Train and tunnel geometries

The geometries of the trains and computational domains used in the present work are discussed in detail in this Chapter. The first part is devoted to the train models and computational domains while the second part is for the tunnel dimensions and shapes.

4.1 Generic train and computational domain

The first part of this study is to examine the methodology used for the computational technique in studying train passing in tunnels. This technique is based on a moving train in a stationary environment. As part of the AeroTRAIN project (Sima et al., 2013), a generic train has been created that has previously been used to investigate pressure pulses in a circular tunnel. The dimensions of generic train, tunnel and computational domain are presented in this Section.

Figure 3 shows the profile of generic train. This profile is described by the following equation;

$$\boldsymbol{h = (S_{tr} + (4r^2 - \pi r^2))/b,} \tag{10}$$

where;

$$\mathbf{S_{tr} = 10m^2,\ b = 3m,\ L_n = 6m,\ r = 0.75m,\ h_0 = 0.25m.}$$

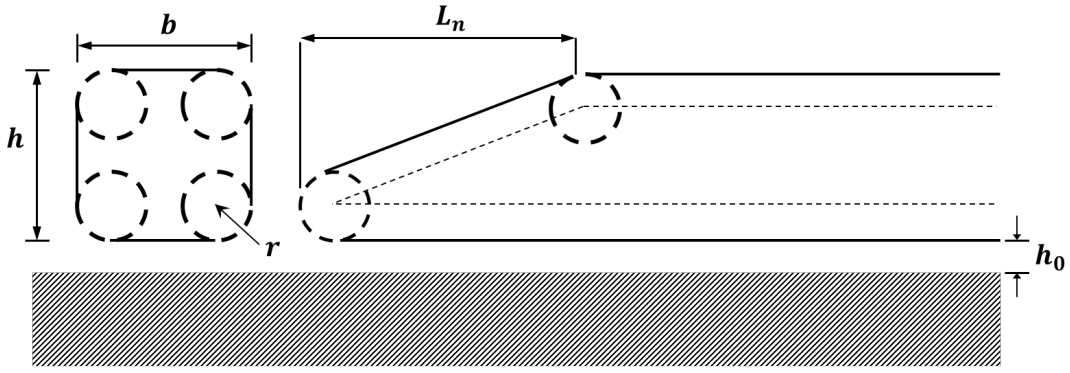

Figure 3. Geometrical illustration of the generic train

Figure 4 shows the dimensions of the generic train used in this thesis. The generic train, tunnel and environment before and after the tunnel are represented in the computational domain (Figure 5).

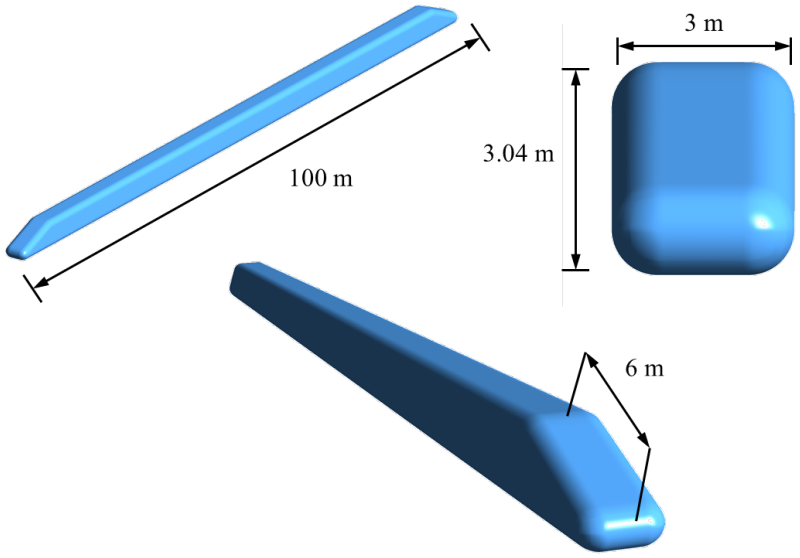

Figure 4. Dimensions of the generic train

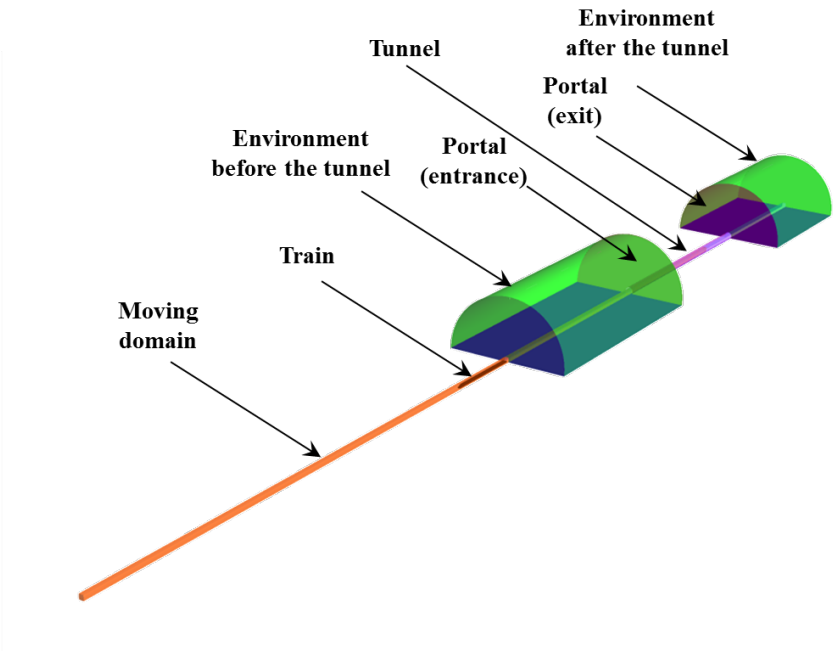

Figure 5 Computational domain of generic train

As shown in Figure 5 the computational domain consists of moving and stationary subdomains. These will be explained later when discussing the computational details. The computational domain also comprises two portals; one at the tunnel entrance and one at the tunnel exit.

4.2 ICE2 train and computational domain

The main train model used in this study is the ICE2 train. The length and cross sectional dimensions of the idealized 1/25th scale ICE2 train model are shown in Figure 6.The ICE2 was chosen as it has received significant attention in the field of train aerodynamics (Gilbert et al., 2013) and is thus useful as a benchmark case. Figure 7 shows the details of inter-carriage gap geometry.

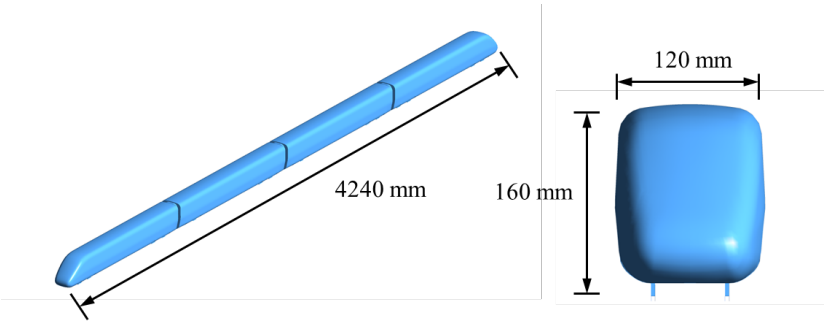

Figure 6 Dimensions of the ICE2 train

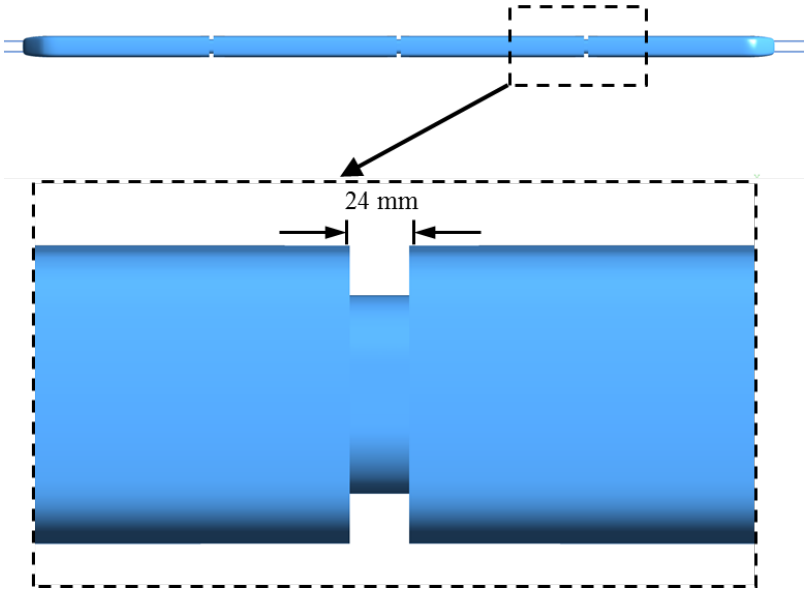

Figure 7. ICE2 inter-carriage gap

The tunnel, the train model and two environments before and after the tunnel form the computational domain of the ICE2 train simulation, shown in Figure 8.

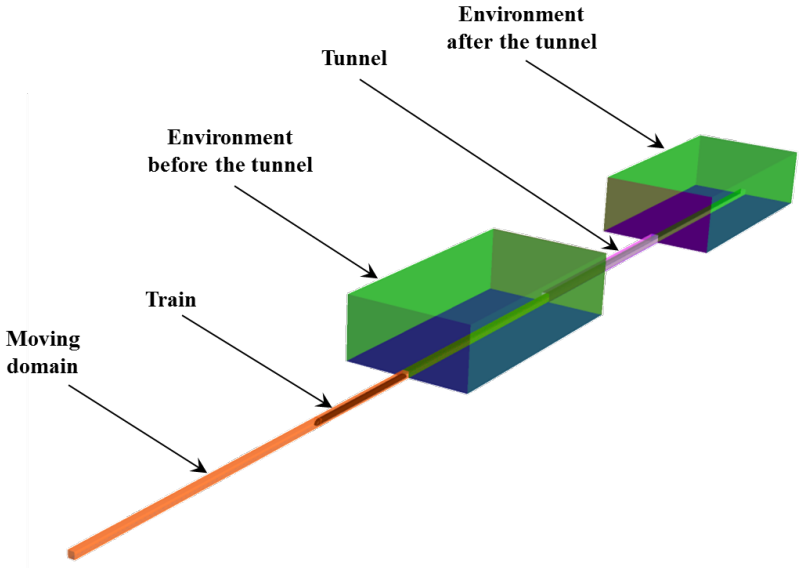

Figure 8. Computational domain for ICE2 train

4.3 Tunnel dimensions and lengths

The three different tunnel cross sections and lengths used in the generic and ICE 2 train simulations are illustrated in the present section.

4.3.1 Generic tunnel

The generic tunnel is of circular cross section with two circular portals. Figure 9 shows the generic tunnel dimensions including; tunnel diameter, tunnel portal diameter and tunnel length. The length of the tunnel is 300m, which is three times the length of the generic train model.

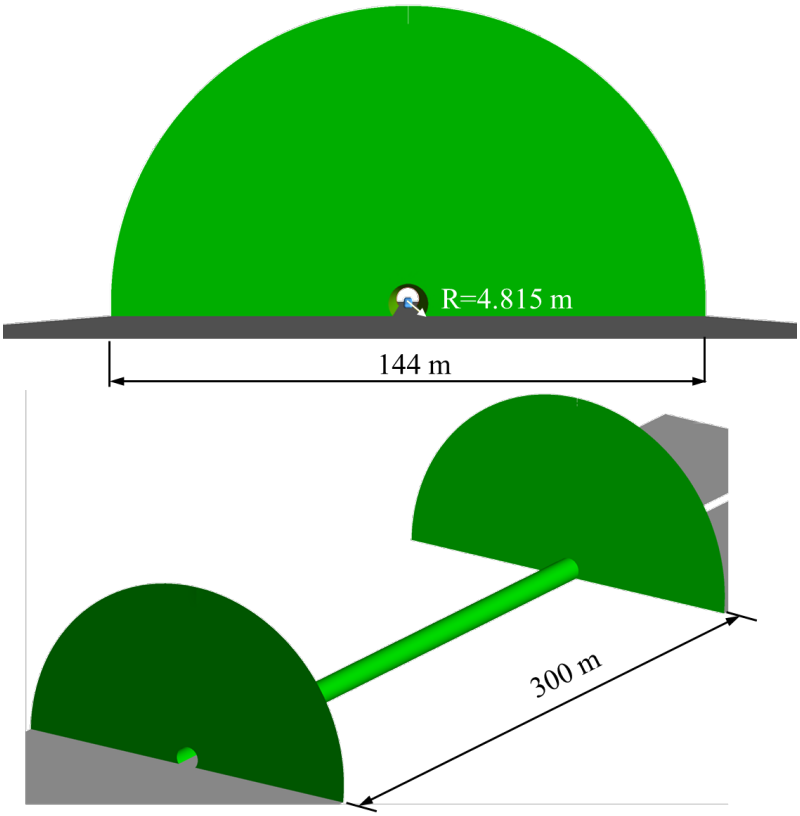

Figure 9 Generic tunnel dimensions

4.3.2 ICE2 Tunnel

The tunnel used in the ICE2 train simulations is of rectangular cross section with no portal at the entrance or exit. Figure 10 shows the ICE2 tunnel dimensions which are similar to those used in the moving train rig experiment of Gilbert et al., (2013). The length of the tunnel is 8m and is called the short tunnel in this thesis. However, another

simulation has been performed on a longer tunnel of 16m length and is called the long tunnel in this thesis.

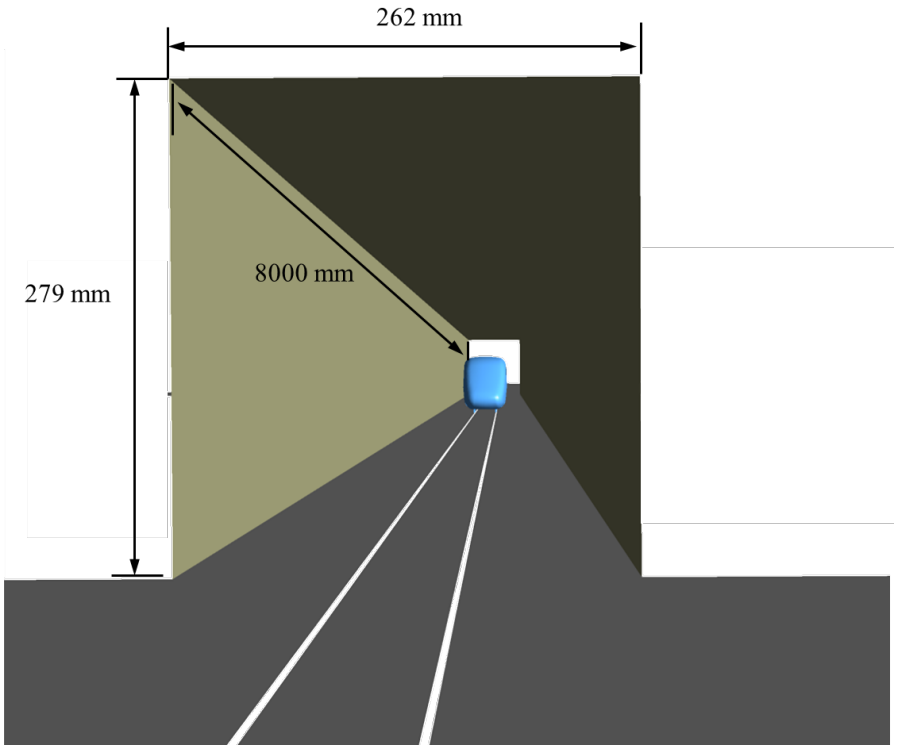

Figure 10 ICE2 tunnel dimensions

Chapter 5. Mesh and numerical details

5.1 Mesh distributions

The commercial software Ansys ICEM-CFD has created all the meshes in this work. Hexahedral meshes were used in all the domains; moving and stationary. Computations were conducted using two different mesh densities for the ICE2 train calculations in the short tunnel. A mesh density similar to the one used for the fine mesh simulations of the short tunnel length was used for the ICE2 train in the long tunnel. The total number of cells for the different simulations is shown in . The same mesh strategy has been used for all the meshes, in which the mesh is concentrated around the train and in the wake region. However, the stretching ratio kept less than 1.2 everywhere.

Table 1. The same mesh strategy has been used for all the meshes, in which the mesh is concentrated around the train and in the wake region. However, the stretching ratio kept less than 1.2 everywhere.

Table 1 Number of mesh cells in the different simulations

Simulation case	Generic	Short tunnel (coarse)	Short tunnel (fine)	Long tunnel
Stationary	3364000	356160	1022112	1060864
Moving	1506848	339032	2336216	2333344
Total	**4870848**	**695192**	**3335828**	**3394208**

Figure 12 shows the mesh distribution around the generic train. The mesh consists of an O-grid inside the moving domain and around the train model. A uniform cell size has been used along the tunnel length while mesh stretching is used on the surface of the train. Mesh densities are greatest close to the nose and tail of the train.

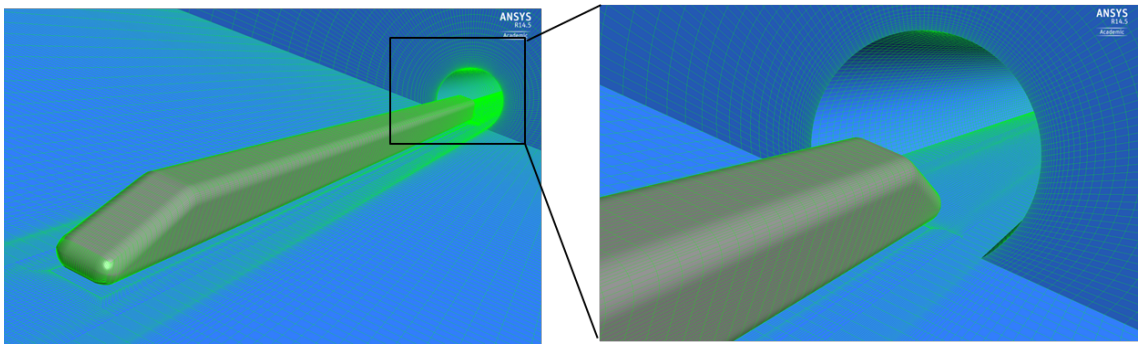

Figure 11 Surface mesh distributions on the generic train model.

Figure 12 and Figure 13 show the mesh distributions around the ICE2 train for the coarse and fine meshes, respectively.

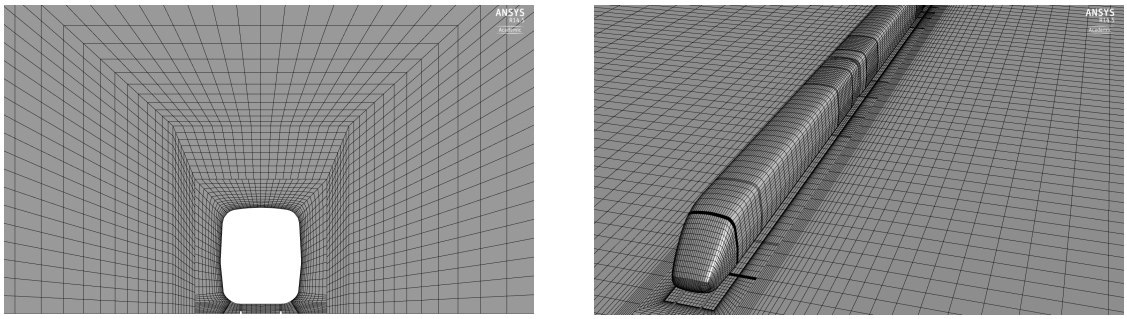

(a) (b)

Figure 12 Coarse mesh distribution around the ICE2 train in the short tunnel simulation

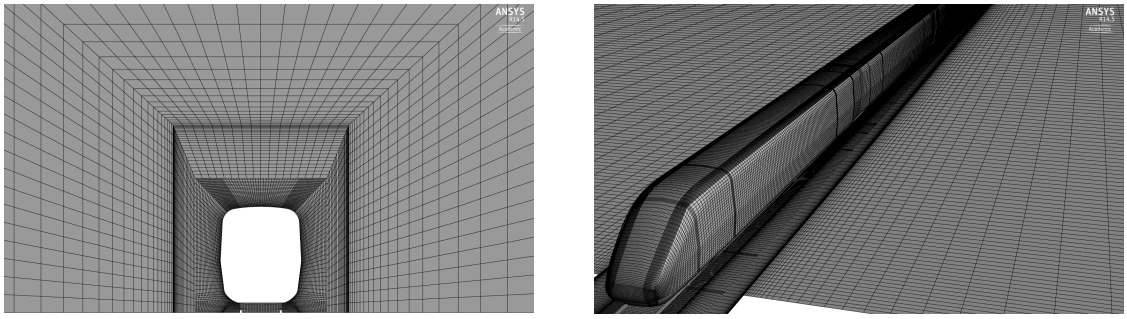

(a) (b)

Figure 13 Fine mesh distribution around the ICE2 train in the short tunnel simulation.

Figure 14 shows the mesh distributions on the symmetry plane. The mesh size has been kept constant inside the tunnel while some mesh stretching has been used along the train

length. The mesh is also concentrated around the nose, tail, inter-carriage gaps and bogies.

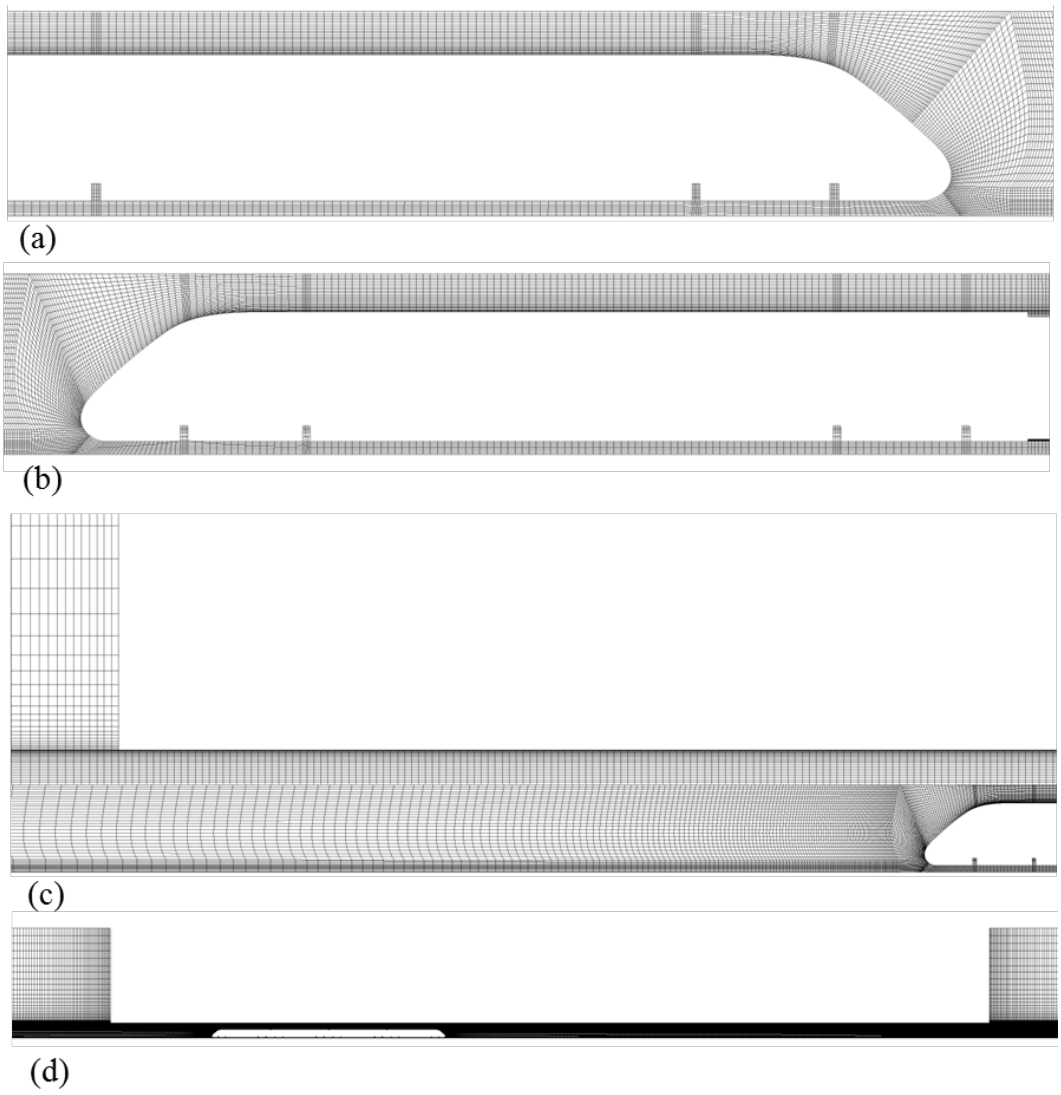

Figure 14 Fine mesh distributions around the train model and inside the tunnel.

5.2 Moving and stationary subdomains

To simulate the movement of the train inside the tunnel, the computational domain is divided into two subdomains; moving and stationary. Figure 15 shows the dimensions of the moving and stationary subdomains. The train model is entirely inside the moving subdomain which is moving relative to the stationary subdomain with the same speed as the train.

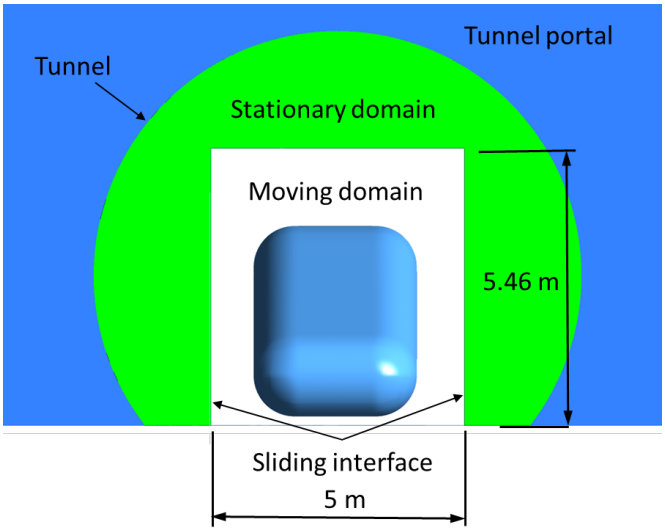

Figure 15 Moving and stationary subdomains.

5.3 Sliding interface

The moving subdomain is inside the stationary domain where the location is updated every time step. In each time step the information (velocity, pressure, turbulence quantities, etc.) are exchanged between the moving and stationary domains through the sliding interface. The position of the sliding interface is shown in Figure 15. The accuracy of exchanging the information through the sliding interface depends on the quality of mesh on both sides of the interface. Thus, special care has been taken to ensure that there is consistency of the sizes of the mesh on the two sides of the interface.

5.4 Boundary conditions

The initial conditions of the simulation were zero pressure and zero velocity in the two domains. The ambient conditions in all cases were set as temperature of 15°C and atmospheric pressure of 101.325 Pa. The entry speed of the train (V_t) was set to 70 m/s for the full-scale generic train and 32m/s for the model ICE2 train. At the beginning of the simulation, the train nose is located at the beginning of the environment. This gives a space for the turbulent flow to develop before the train arrives to the tunnel portal. No-slip boundary conditions were applied to the train surface, tunnel, portals and the ground of the stationary domain. A moving-wall boundary is applied on the ground of the

moving subdomain. Convective boundary conditions are applied on the top, sides and ends of the environments and all the walls were assumed adiabatic.

5.5 Discretization schemes

The conductive terms in the governing equations were discretised in space using the second order central-differencing scheme while the convective schemes were discretised using the high-resolution scheme in CFX, which is a second order scheme in space. The time step was 0.0001 second in all the simulations of the ICE2 train and 0.0015 second for the generic train. The total simulation time allowed for the tail of the train to be at least 3 m from the exit of the tunnel in case of the small scale model and 100 m from the tunnel exit for the generic train simulation.

Chapter 6. Results

In order to investigate the effect of the tunnel length on the velocity and pressure around train passing through a tunnel, the following simulations were performed: generic train passing through a single tunnel, a simplified ICE2 train passing through a short tunnel and a simplified ICE2 train passing through a long tunnel. Details and results from each simulation are described in the following Sections.

6.1 Generic train simulation

Figure 16 shows the position of the monitoring points in relation to the tunnel entrance. For the generic train simulation only the pressure data was monitored at static points at 100 m (x=100 m) from the entrance (P3, P4, P7 in Figure 16). The coordinate system is shown in Figure 16 and Figure 17. The y-z coordinates of three points are shown in Figure 17. The monitoring point P3 is located inside the moving domain, 2m from the centre of the tunnel and 5 m from the top of the rail, whilst P4 is located at the same height as P3 but in the stationary domain (3m from the centre of the tunnel). This is to ensure that the flow information is exchanged properly between the stationary and moving domains. Probe P7 is at the same distance from the tunnel entrance and the same distance from the centre of the tunnel as P4. This point is to investigate whether any pressure difference occurs at the same cross-sectional position in the tunnel.

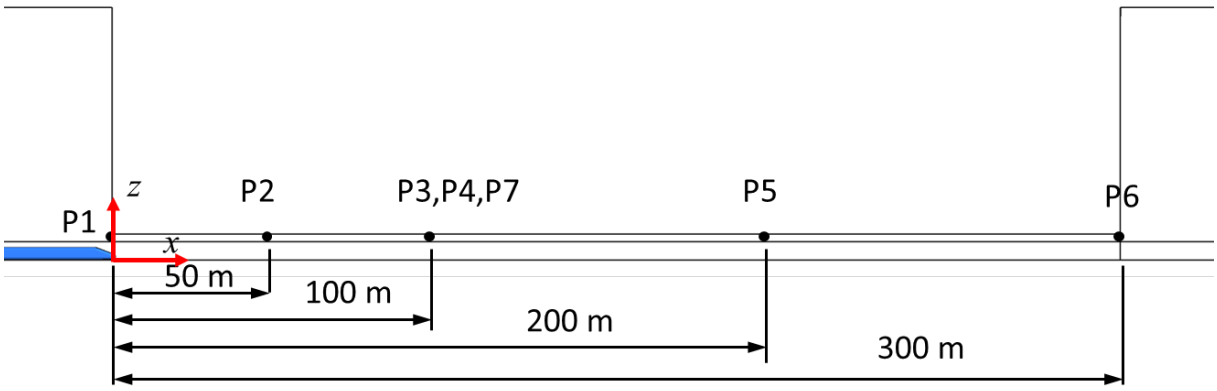

Figure 16 The positions of monitoring points along the tunnel

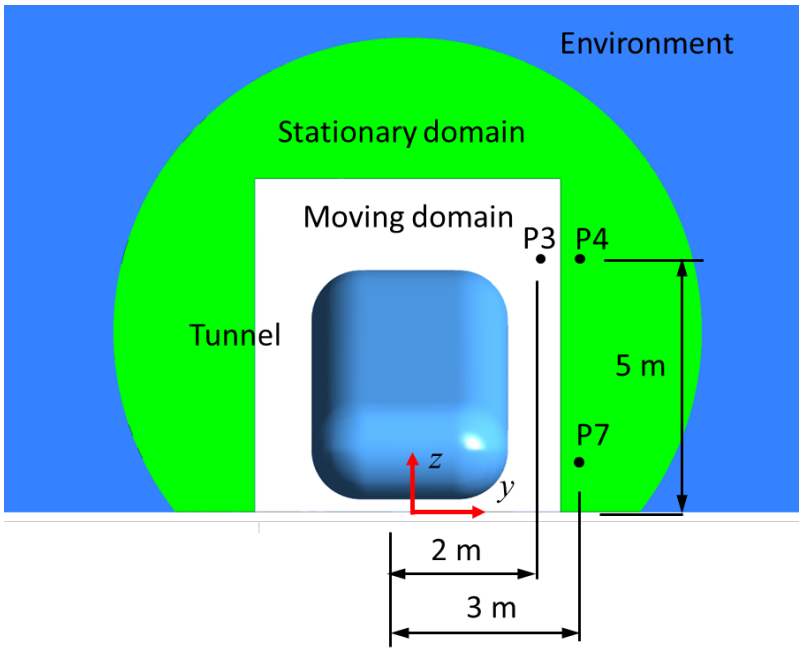

Figure 17 The location of P3, P4 and P7 monitoring points

Figure 18 shows the time history of the pressure at P3, P4 and P7 during the simulation. The three pressure curves show quite similar magnitudes, which suggest a proper exchange of data between the stationary and the moving domains. Figure 18 shows also that the pressure data at P7 is quite similar to the pressure data at both points P3 and P4 meaning that the pressure field is the same at the same cross section.

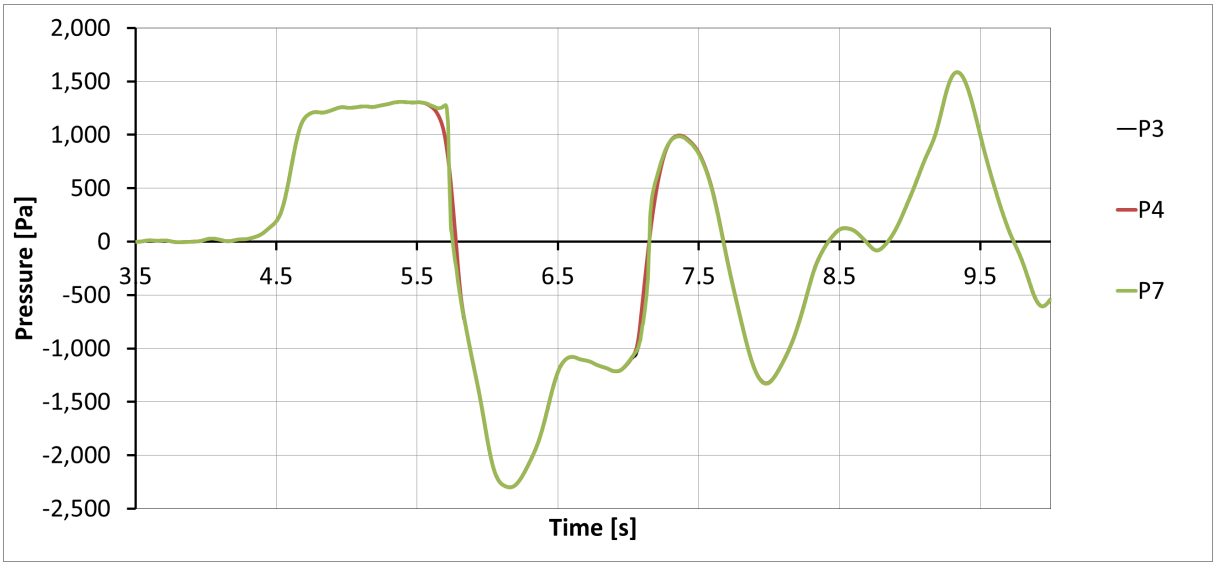

Figure 18 Pressure data history for P3, P4 and P7 monitoring points during the generic train simulation

In the AeroTRAIN project, the pressure data were obtained at point P3 on a similar tunnel and a generic train. The pressure data have been obtained by different organisations using different CFD packages and different meshes. In order to reduce the simulation costs for these companies, the AeroTRAIN simulations were stopped after 0.8 s, after the train enters the tunnel. All the simulations from the AeroTRAIN agreed that the pressure at point P3 reaches approximately 1200 Pa when the train enters the tunnel (corresponds to about 4.7 s from the start of the simulation) and then increased up to 1250 Pa at about 0.8 s after the train enters the tunnel. It can be seen from Figure 18 that the CFD results agree very well with those from the AeroTRAIN data. When the train head approaches the measurement point, the pressure drops to -2250 Pa and after the nose of the train passes the point large fluctuations were obtained in the pressure. These fluctuations can be related to the nature of the ideal gas media as it will be seen later in this report that these fluctuations disappear in case of air at 25^{o}.

Figure 19 shows the change of pressure with time (pressure gradient) at the monitoring point P3. Similar results were obtained in the AeroTRAIN project thus providing some validation to the CFD simulations. The figure shows large gradients at the monitoring point, p3, when the train enters the tunnel, when the head of the train approaches the point, when the tail of the train is passing the point and when the train leaves the tunnel which correspond to 0 s, 1 s, 3.3 s and 3.8 s from the moment the train enters the tunnel,

respectively. Some fluctuations after the train leaves the tunnel can be observed until the pressure stabilises to atmosphere pressure.

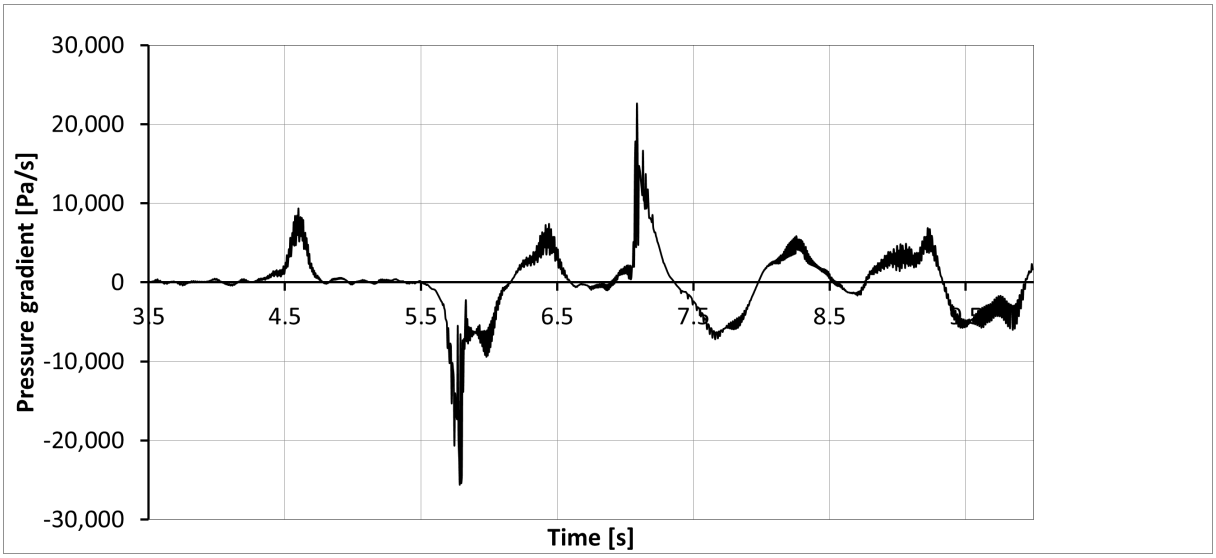

Figure 19 Change of pressure with time at point P3

It is important to correctly calculate the magnitude of the pressure gradient as it, to a large extent, determines the strength of micro pressure waves at the exit of the tunnel. Although it is important to determine the static pressure inside the tunnel, the magnitude of pressure gradient is more important for evaluating the passenger comfort and fatigue of the train body.

Figure 20 shows the static pressure at different points along the length of the tunnel at different distances from the tunnel entrance. All the points show similar pressure variation but with different pressure magnitudes. This means that the pressure variations inside the tunnel are due to specific effect of the position of the train such as the entrance of the nose and tail. Also there is a pressure drop inside the tunnel demonstrated by the different pressure magnitudes.

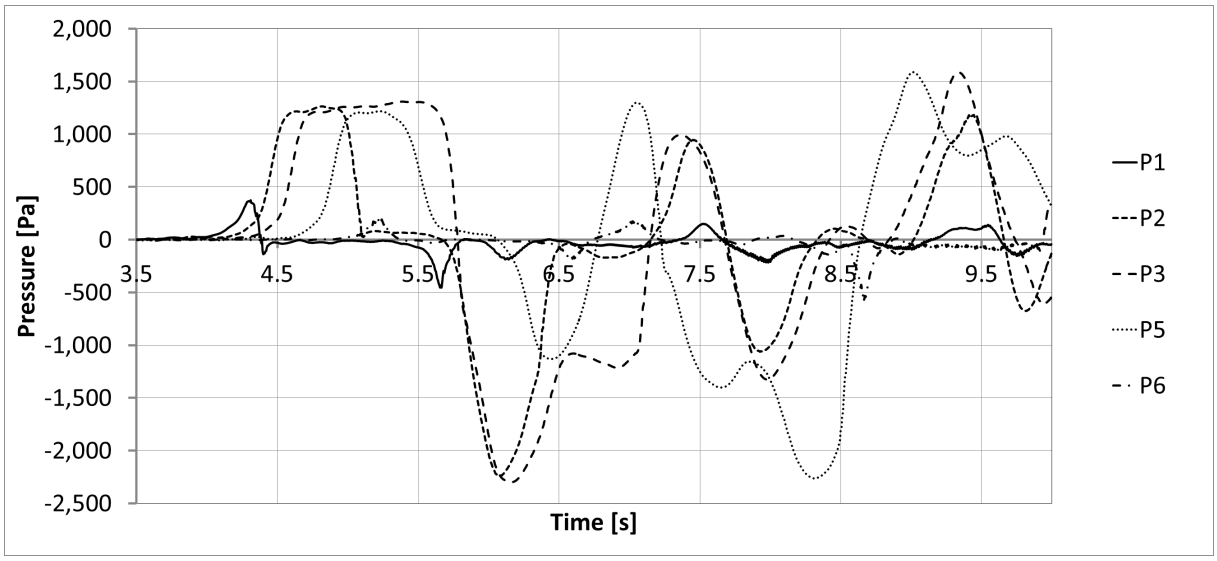

Figure 20 History of static pressures at the monitoring points.

Figure 21 shows the pressure gradient obtained at the same points as in Figure 20. The figure shows that the profiles of the pressure gradients are very similar for all measurement positions. However, different magnitudes of both peaks and troughs are observed from the different points with different in the occurring time corresponding to the speed of the train.

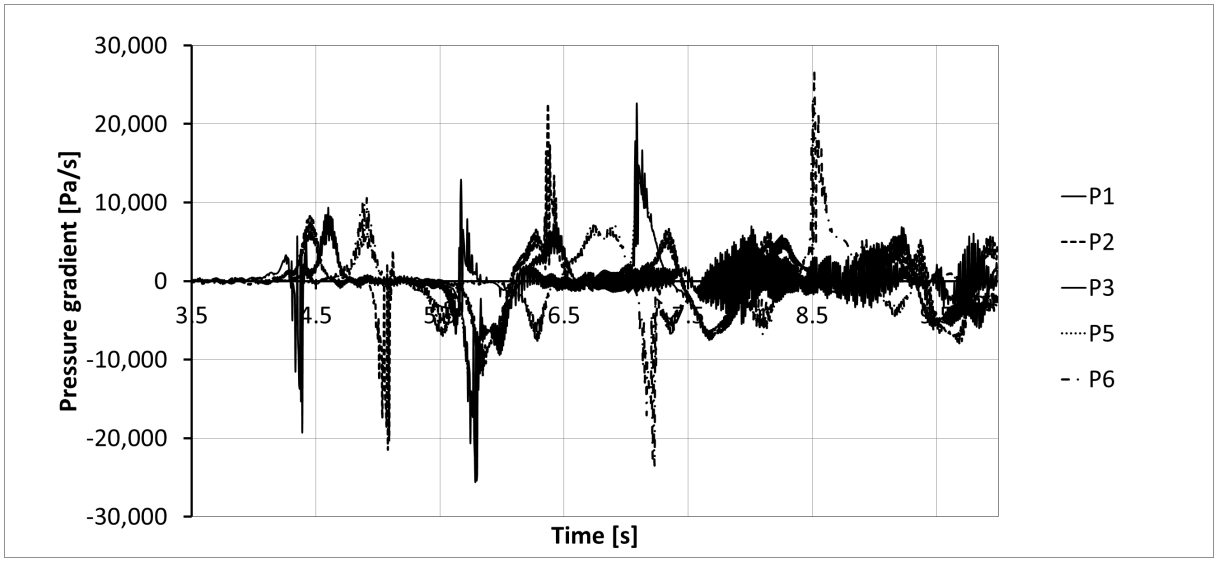

Figure 21 History of the pressure gradients at the monitoring points.

6.2 ICE2 train passing a short tunnel

In this section, the results from the simulation of the ICE2 train entering a short tunnel are presented. The data include; static pressure, the pressure gradient and the flow around the train and inside the tunnel.

6.2.1 Mesh sensitivity and numerical validation

Figure 22 shows the cross sectional profile of the ICE2 train in the tunnel. The figure shows also the locations of the monitoring points used in Gilbert et al., (2013) to obtain the slipstream velocities.

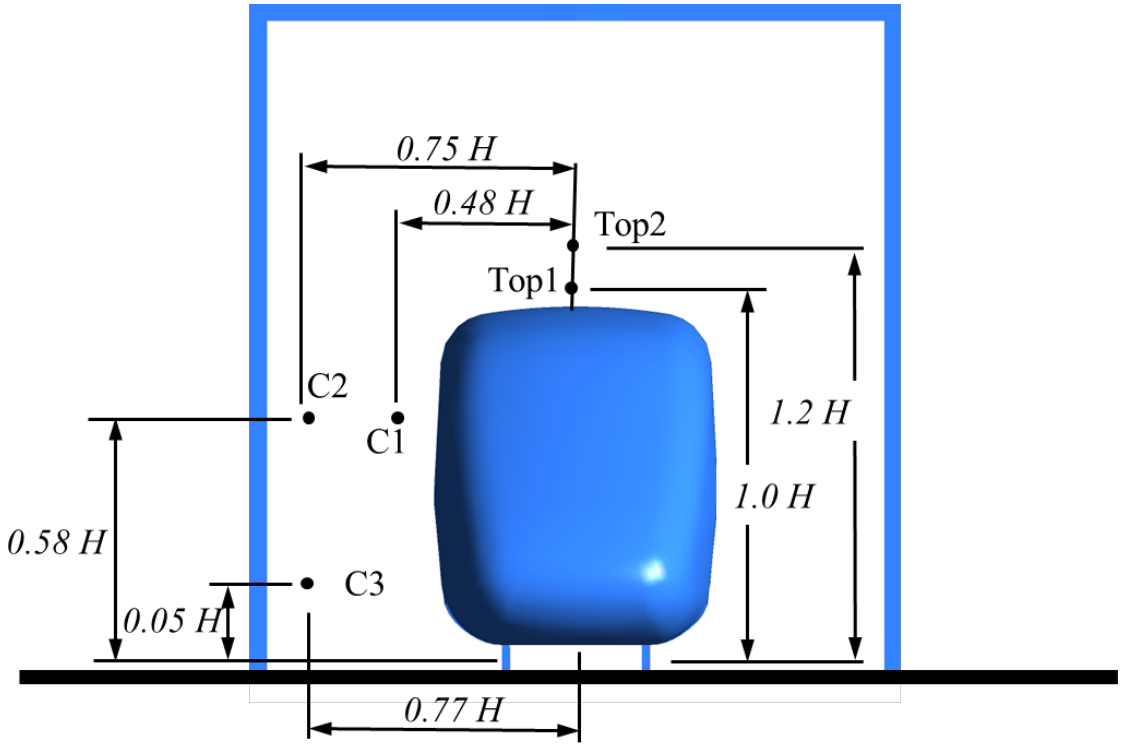

Figure 22 Cross section of the train and tunnel showing the monitoring points of the experimental work.

Figure 23 shows the velocity magnitude at the monitoring point C3 normalized by the train speed as a function of the distance between the point and the nose of the train. The data are presented from fine and coarse meshes together with the experimental data from Gilbert et al., (2013).

Both the fine and coarse meshes give the similar results ahead and along the train length however, larger discrepancies occur behind the train. Both the fine and coarse meshes

show a similar trend to the experimental data. There is however a large discrepancy between the numerical and the experiment results for the location of the peak gust in the wake behind the train; for the experiment it occurs at S/H=35, for the fine mesh it occurs at S/H=37 and for the coarse mesh it occurs at S/H=40, where S is the distance between the monitoring point and the nose of the train and *H* is the train height.

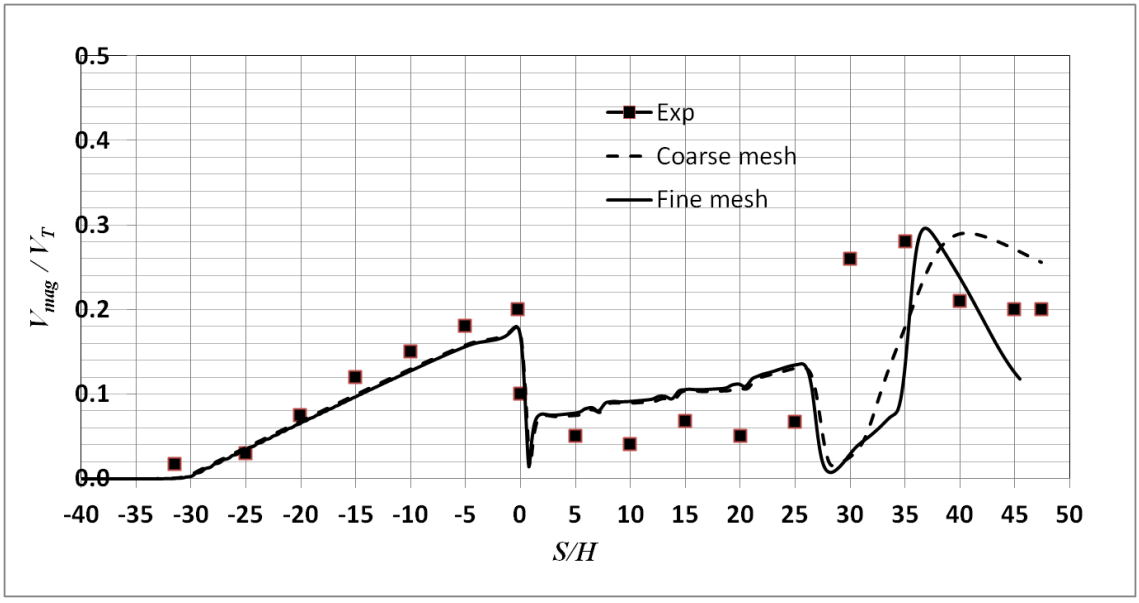

Figure 23 Normalised velocity magnitude as a function of the distance between the nose of the train and monitoring point C3.

Figure 24 shows the experimental data from Gilbert et al., (2013). The solid lines represent the ensemble average while the symbols show locations of gust peaks. The gust peaks always occur in the wake behind the train. However, there is a large scatter in the location of the gust peaks from run to run, where they occur between 27<S/H< 47. The highly-turbulent nature of the flow behind the train causes difficulty in obtaining good agreement between the location of the peak gusts in both experimental and numerical works.

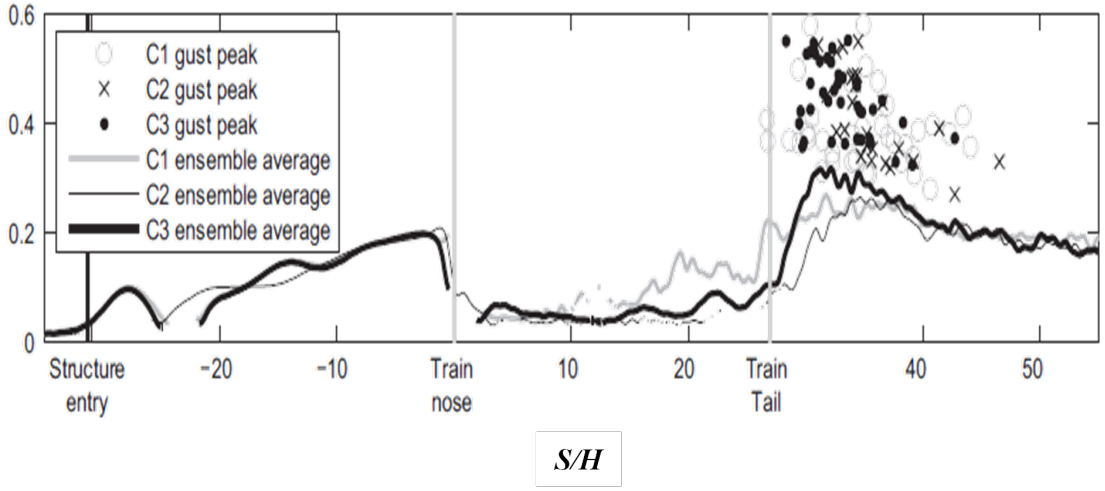

Figure 24 Data from model-scale experiments (Gilbert et al., 2013).

A difference is also observed between the experiment and CFD along the length of the when the train is passing the point. To explain this difference, Figure 25 shows the velocity magnitude and longitudinal component together with the velocity magnitude from the experiment. It can be seen that the longitudinal velocity component is negative when the train is passing the measurement point.

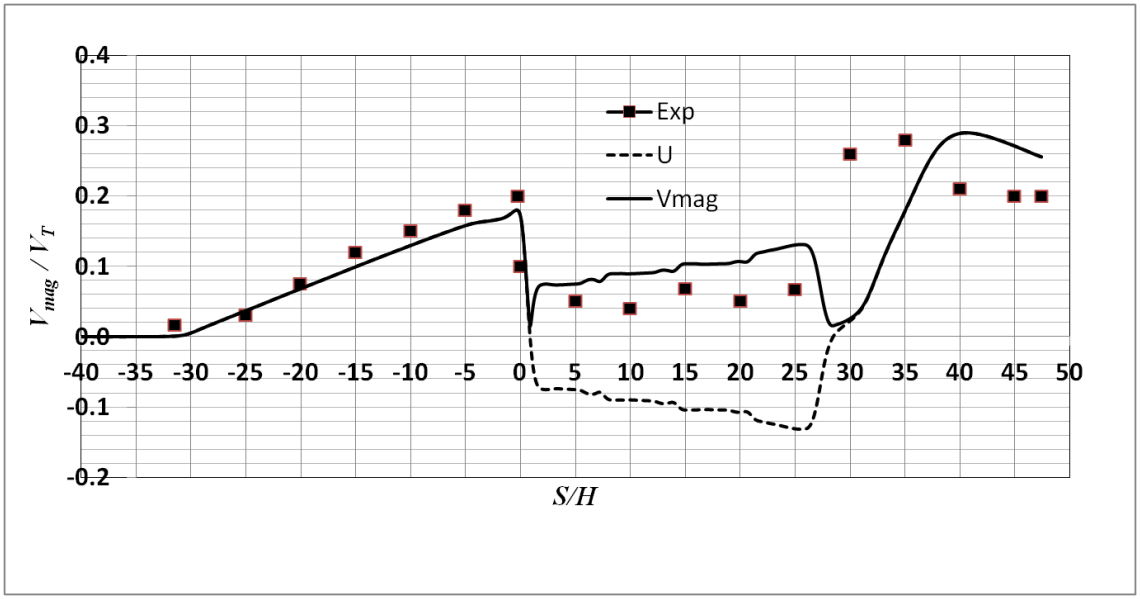

Figure 25 Comparison between the velocity magnitude and the velocity component at the monitoring point C3.

The velocity has been measured in the experiment using a Cobra probe and it is known that this kind of device is unable to measure a reverse flow thus the discrepancy between the results can be related to this limitation of the measurement equipment. Also this dicrepancy can be related to the possibality that the RAN simulation is unable to correctly predict the region of seperation and re-attachment around the train.

6.2.2 Air velocity in the tunnel

Figure 26 shows the histories of the velocity magnitude at points C1, C2 and C3, shown in Figure 22. Similar to Figure 26, Figure 27 shows the longitudinal velocity component at the three points.

When the train approaches the points the same velocity magnitude and velocity component are measnred at all points. The maximum velocity magnitude is about 18% of the train velocity when the head of the train arrives at the section of the monitoring points.

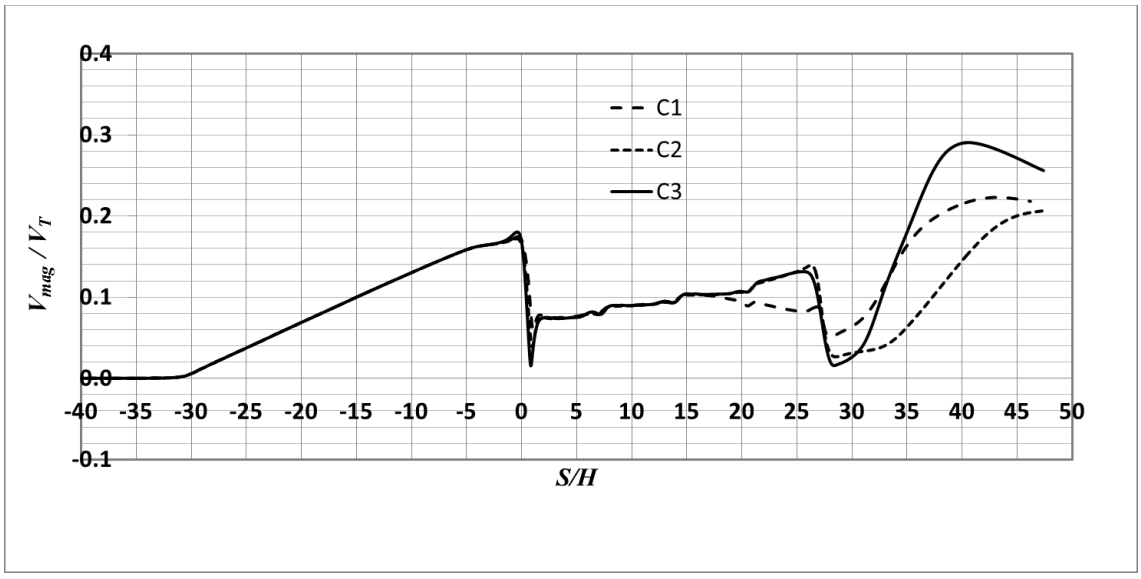

Figure 26 Short tunnel; Velocity magnitude at points C1, C2 and C3 shown in Figure 22.

The velocity component ahead of the train is similar to that of the velocity magnitude suggesting that the other lateral and vertical velocity components are negligible. Figure 28and Figure 29 show the history of the spanwise and vertical velocity components at the three points. It can be seen that these two components have zero velocity before the train

head approaches the section of the monitoring points. There are some changes in these two components when the train head passes but the magnitude of these components is very small in comparison to the longitudinal velocity component.

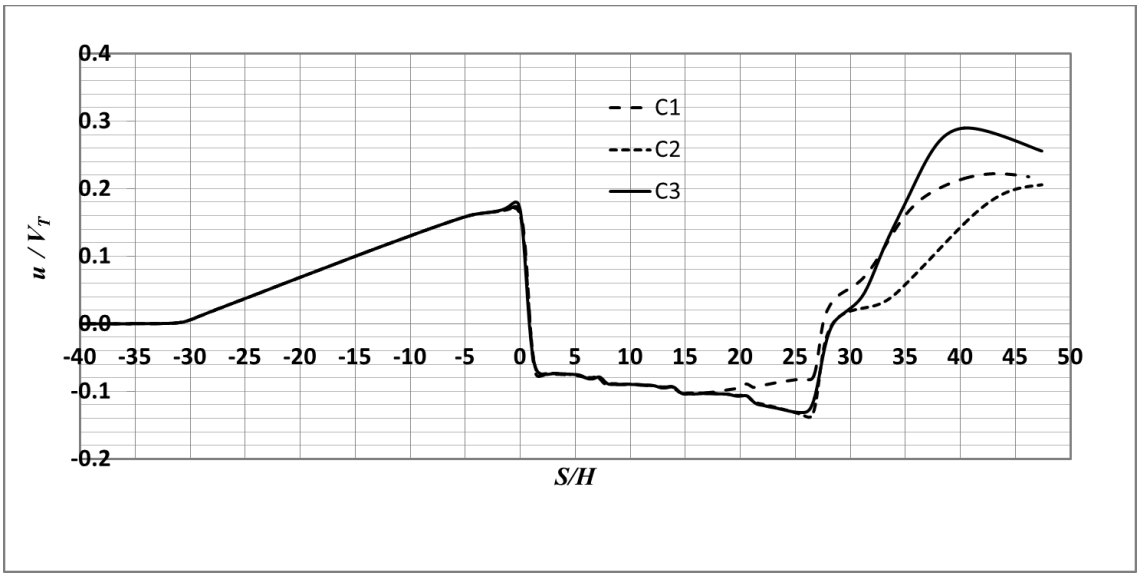

Figure 27 Short tunnel; Velocity component in direction of travel at points C1, C2 and C3 shown in Figure 22.

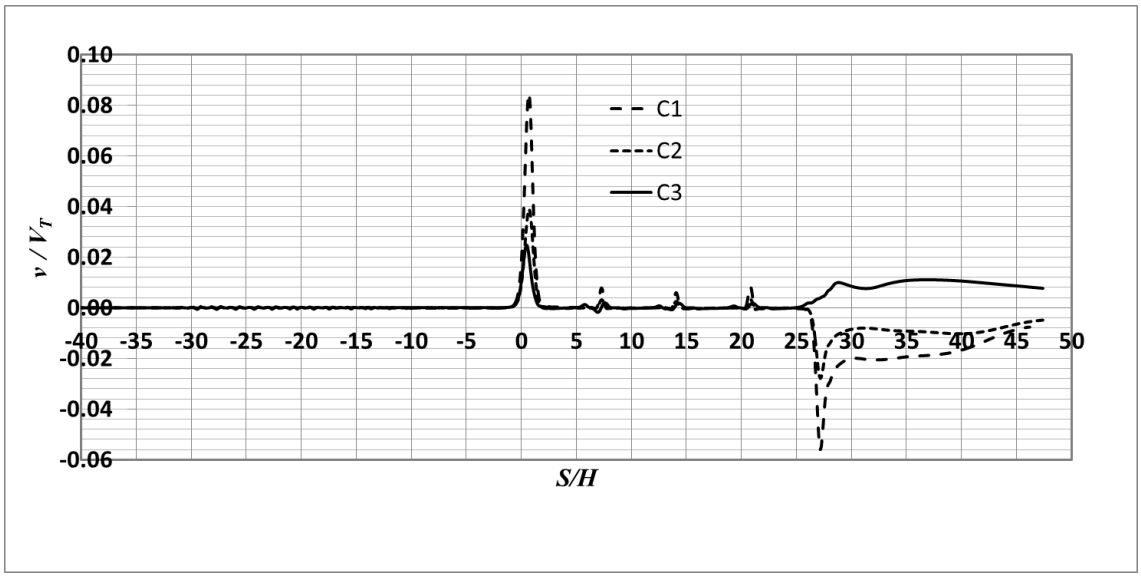

Figure 28 Short tunnel; Velocity component in the span-wise direction at points C1, C2 and C3 shown in Figure 22

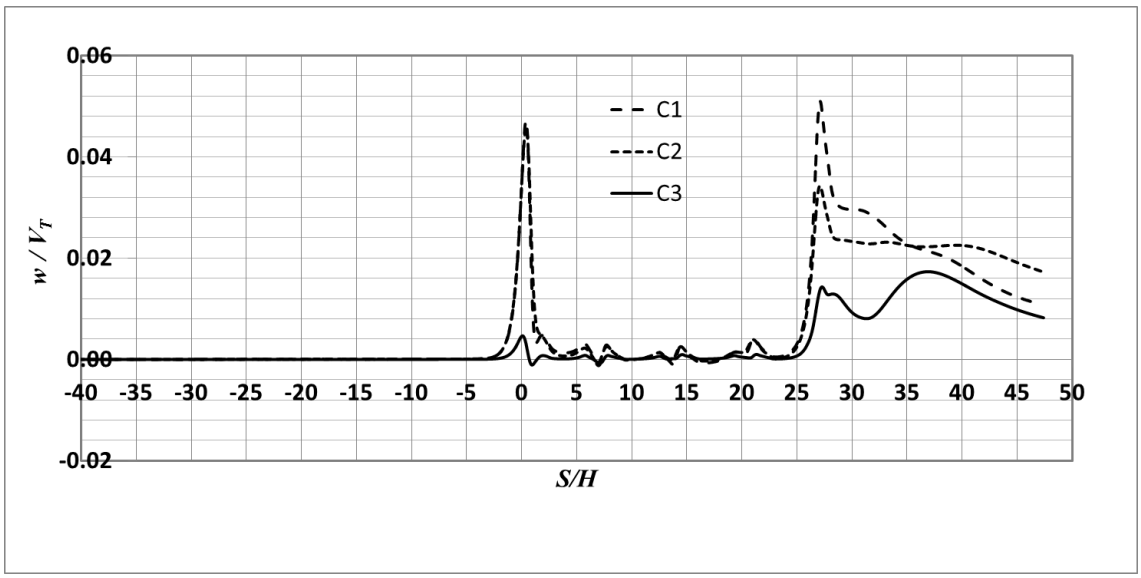

Figure 29 Short tunnel; Velocity components in the vertical direction at points C1, C2 and C3 shown in Figure 22

Similar behaviour can be seen in the velocity components along the length of the train at which the velocity magnitude is similar to the longitudinal velocity component. The significant effect of the spanwise and vertical velocity components is clear at the wake of the train and at the inter-carriage gaps where some the most prominent lateral velocity components are observed.

Figure 26 show that the three points have the same velocities ahead and along the first three cars of the train. Along the length of the last car, point C1 (closest to the train surface) has a lower velocity magnitude that the other two points. Figure 27 shows that the longitudinal velocity component is negative at the three points i.e. the flow is reversed. As point C1 is the closest to the train surface, the velocity is affected by the boundary layer region of the train slipstream and thus has less reversed flow than the other two furthest points.

It can be seen also from Figure 26 that in the wake flow, point C3 has the maximum velocity followed by point C1 and then C2. This is because C3 is close to the ground and in this region the flow is affected by the underbody complexities. Also C1 is close to the train surface i.e. maximum slipstream effect.

Figure 30 and Figure 31 show the longitudinal velocity component and magnitude, respectively at points Top1 and Top2 shown in Figure 22.

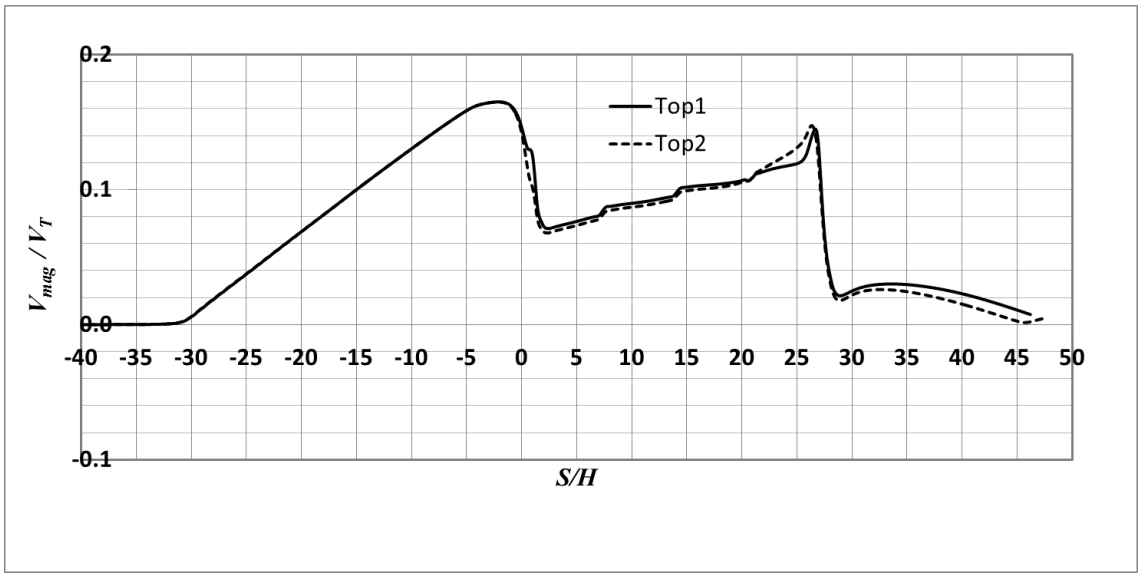

Figure 30 Short tunnel; Velocity magnitude at points Top1 and Top2 shown in Figure 22

Similarly to the velocities at points C1, C2 and C3, the velocities above the train are comparable ahead and along the first three cars of the train. Along the length of the last car, the furthest monitoring point from the surface of the train (Top2) has a larger velocity than the closest one (Top1). This behavior is due to reversed flowin the wake as was observed for points C1, C2 and C3.

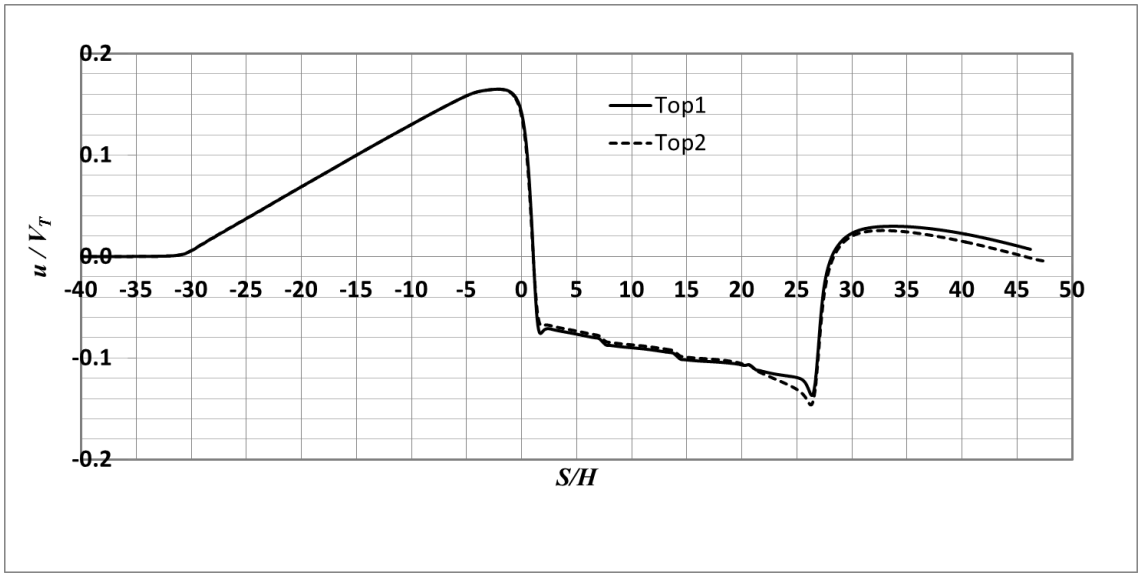

Figure 31 Short tunnel; Velocity components in direction of travel at points Top1, and Top2 shown in Figure 22

When the train enters the tunnel, a large vortex occurs at the front of the tunnels as the train drags air from the outside, into the tunnel. Some of this air comes from the environment above the tunnel to form a large circulation region as shown by the second invariant of the velocity gradient tensor in Figure 32 and the streamlines in Figure 33.

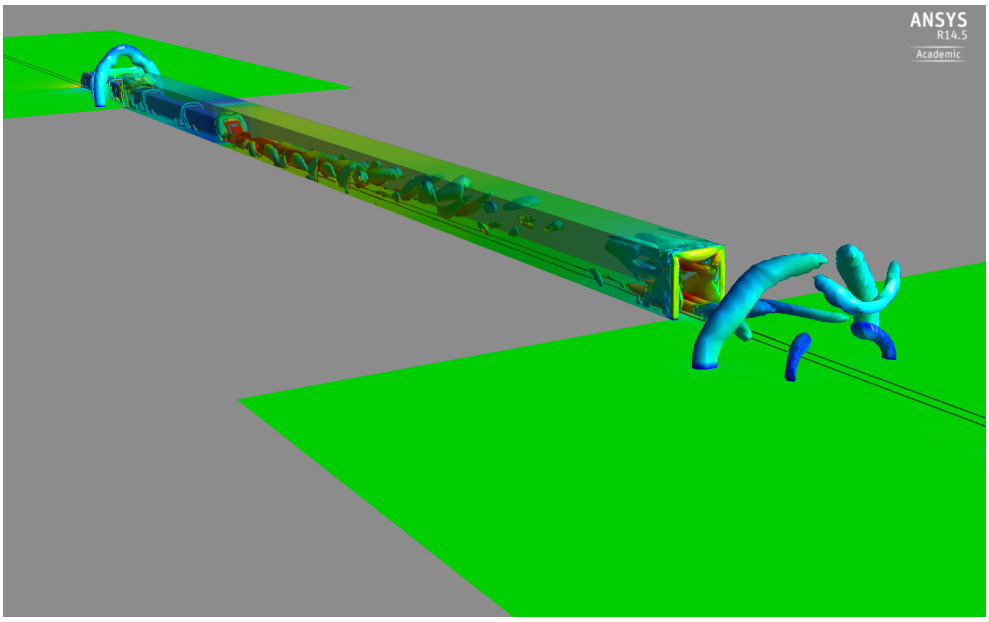

Figure 32 Short tunnel; Second invariant of the velocity gradient tensor in the short tunnel showing the large vortex at the tunnel entrance.

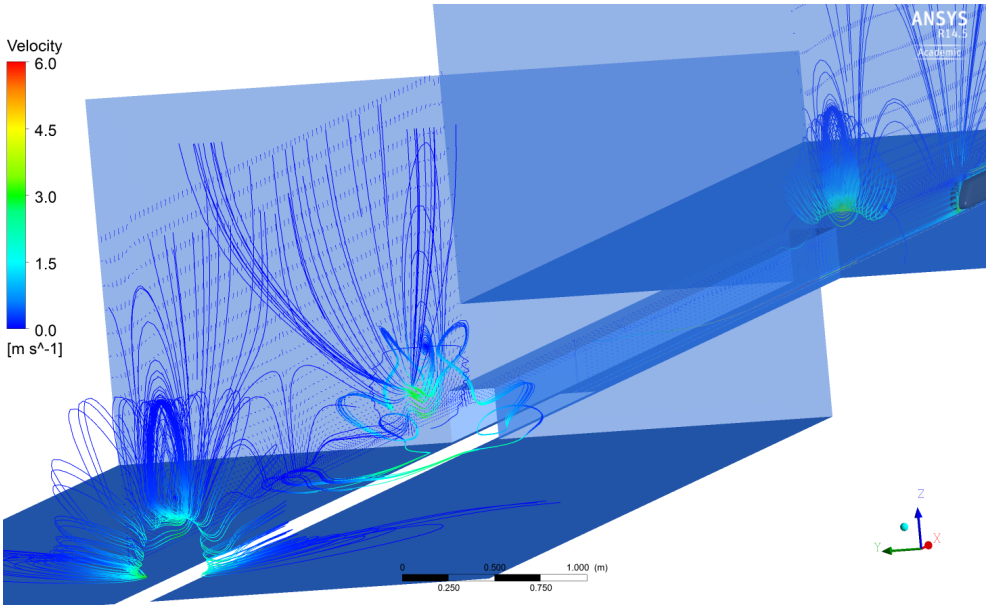

Figure 33 Short tunnel; Three-dimensional streamlines showing the large vortices at the entrance and exit of the short tunnel.

Similar to the wake flow outside the tunnel, two trailing vortices are observed behind the train. These two vortices are shown in Figure 34 using the second invariant of the velocity gradient tensor. The direction of the air rotation in these two vortices is shown in Figure 35 using the velocity vectors.

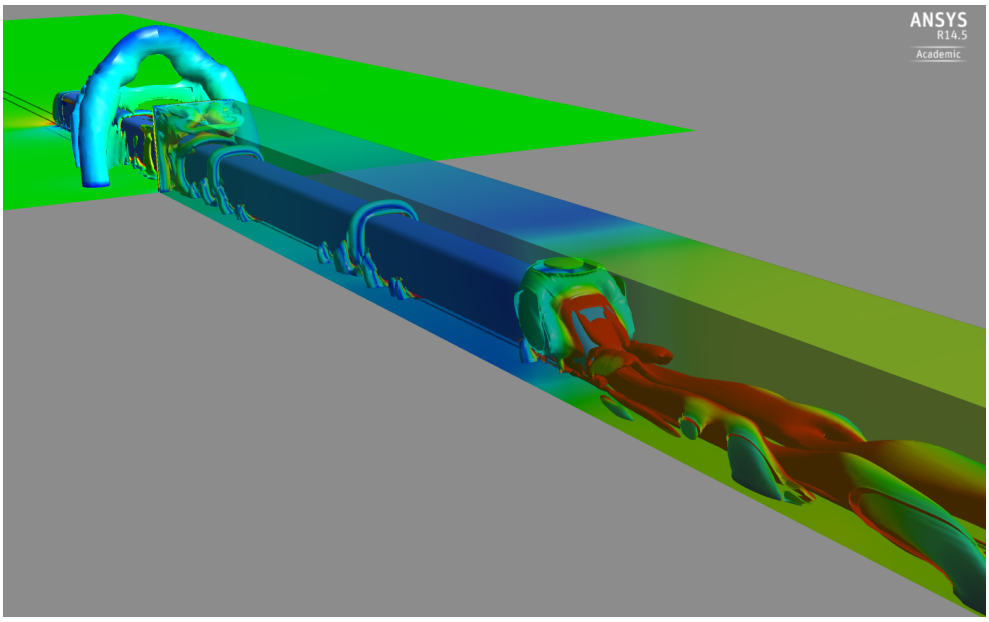

Figure 34 Short tunnel; Second invariant of the velocity gradient showing the two trailing vortices inside the tunnel.

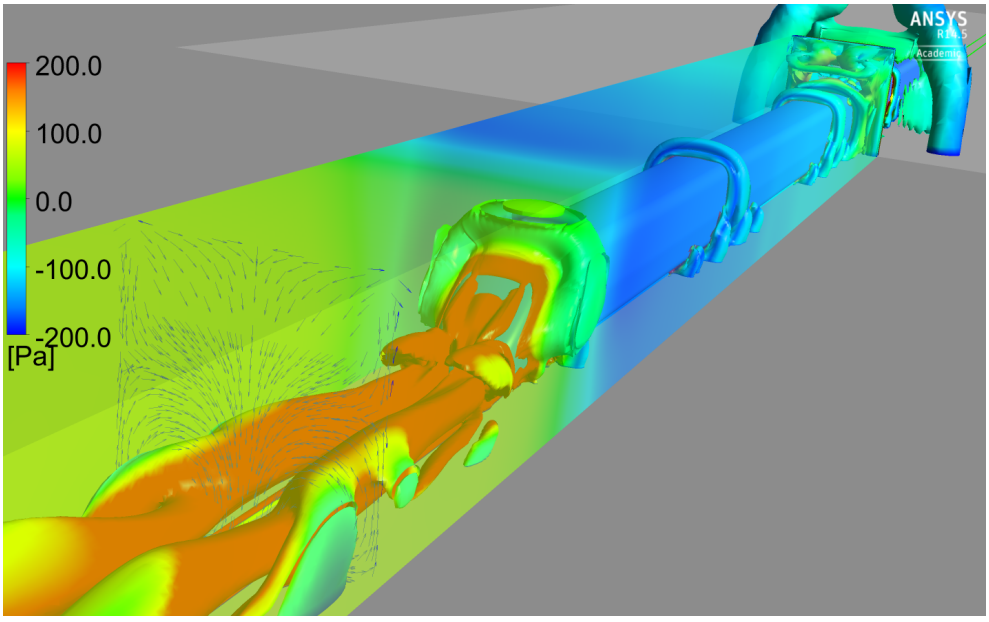

Figure 35 Short tunnel; Second invariant of the velocity gradient and velocity vectors showing the rotation of the trailing vortices.

Inside the tunnel, the air is dragged behind the train while in the region around the train the air moves backward towards the wake flow. This is due to the high pressure ahead of the train and the low pressure in the wake. This is shown in Figure 36 in terms of velocity vectors projected on the symmetry plane. It can also be seen in Figure 36 that the air very close to the train surface moves at the same direction of the train whilst the air further from the train moves in the opposite direction.

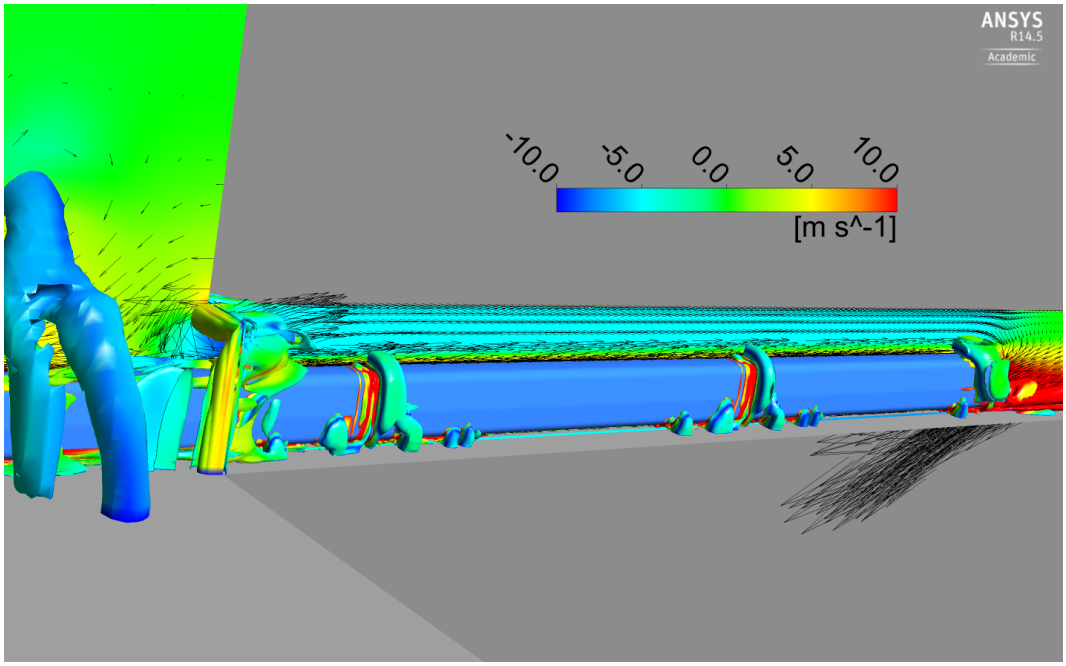

Figure 36 Short tunnel; Second invariant of the velocity gradient and velocity vectors showing the direction of the air inside the tunnel around the train.

Once the train leaves the tunnel a similar large vortex to the one observed at the entrance occurs at the tunnel exit. This vortex is shown in Figure 37 using the second invariant of velocity gradient tensor and in Figure 38 using the three-dimensional streamlines. The direction of air rotation within this vortex is shown in Figure 39.

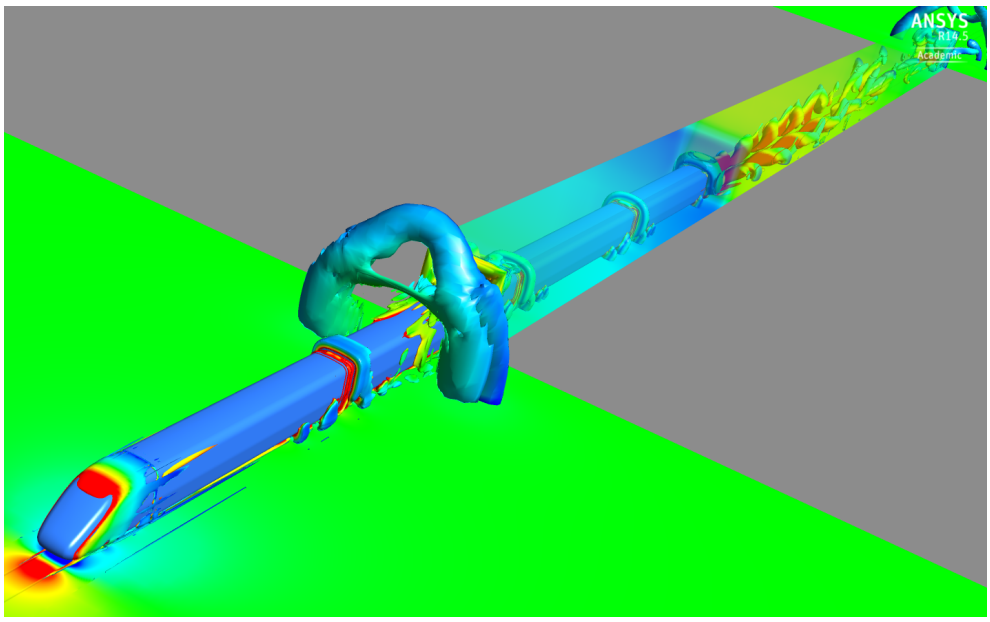

Figure 37 Short tunnel; Second invariant of the velocity gradient showing the large vortex at the tunnel exit.

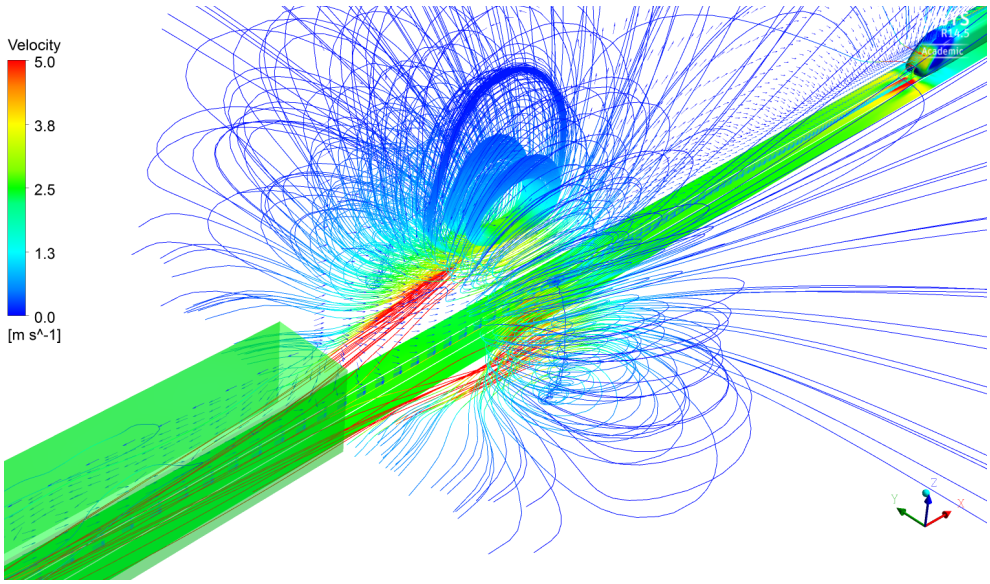

Figure 38 Short tunnel; Three-dimensional streamlines and velocity vectors showing the large vortex at the tunnel exit and the direction of the air inside the tunnel after the exit of the train.

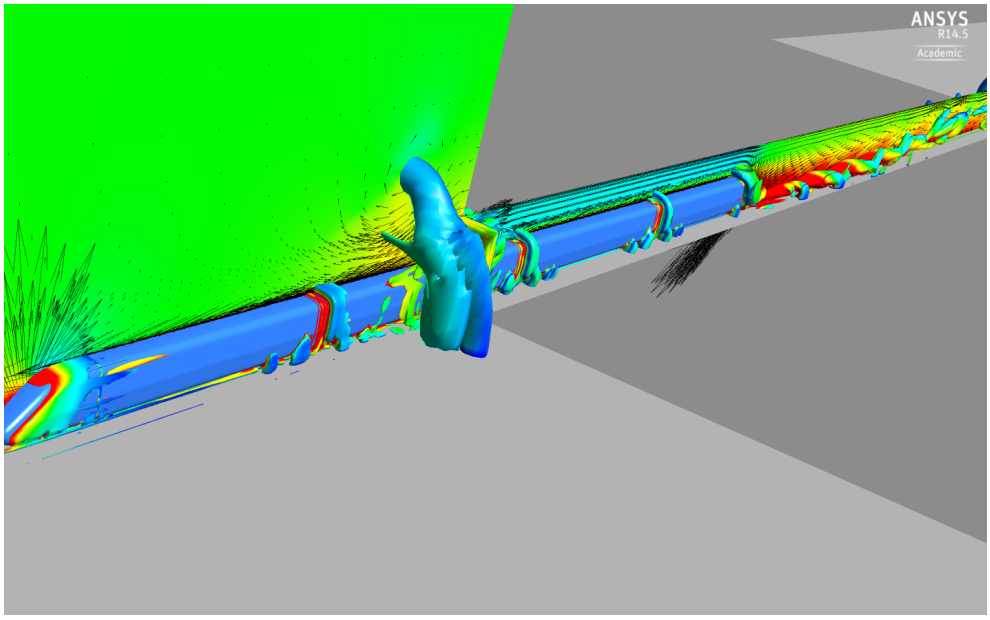

Figure 39 Short tunnel; Second invariant of the velocity gradient and velocity vectors showing the rotation of the large vortex at the tunnel exit.

6.2.3 Pressure in the tunnel

The static pressure inside the tunnel was monitored during the simulation at four different points; P1, P2, P3 and P4 as shown in Figure 40. Point P1 is at the tunnel entrance and P4 is at the tunnel exit. Points P2 and P3 are positioned at one third and two thirds along the length of tunnel, respectively. The four points are at 0.77H from the centre of track and at 1.12H from the top of rail.

Figure 41 shows the history of the static pressures at the four points as a function of the distance between the train nose and the tunnel entrance. Before the train nose enters the tunnel, the static pressure at the four points is zero. Once the train nose enters the tunnel, a sharp increase in the pressure occurs at points P1, P2 and P3, while the pressure at P4 is remains at zero. This is because P4 is at the exit of the tunnel and is influenced by the static pressure of the exit environment.

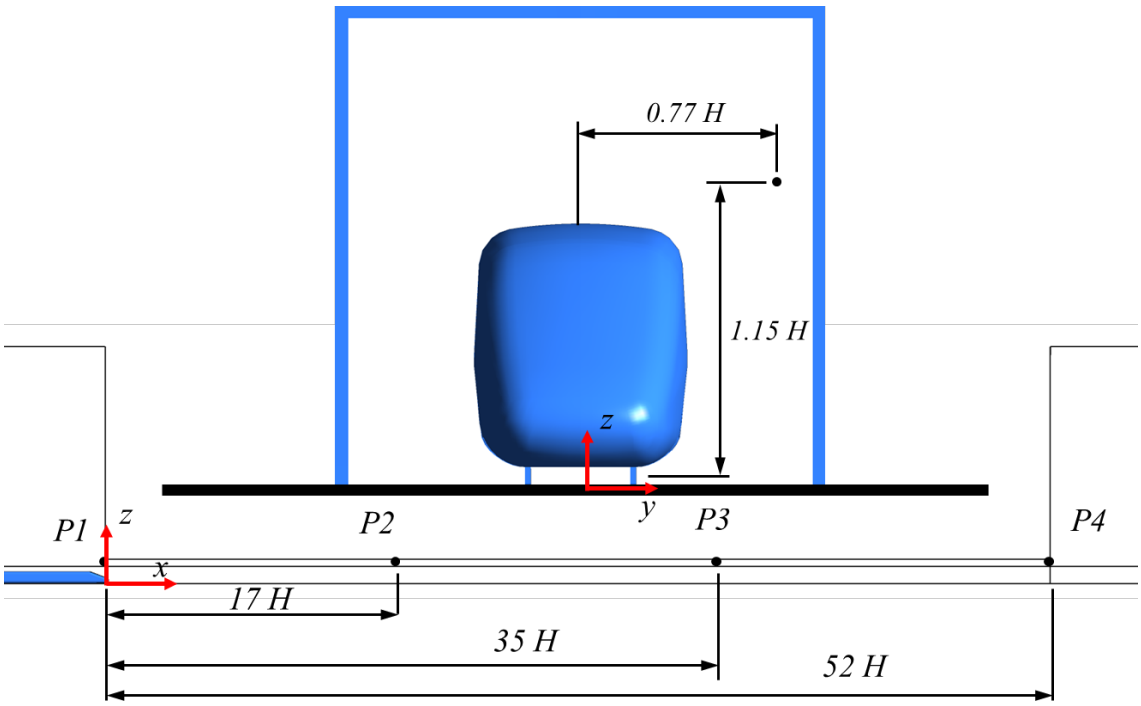

Figure 40 Schematic diagram showing the monitoring points for the static pressure.

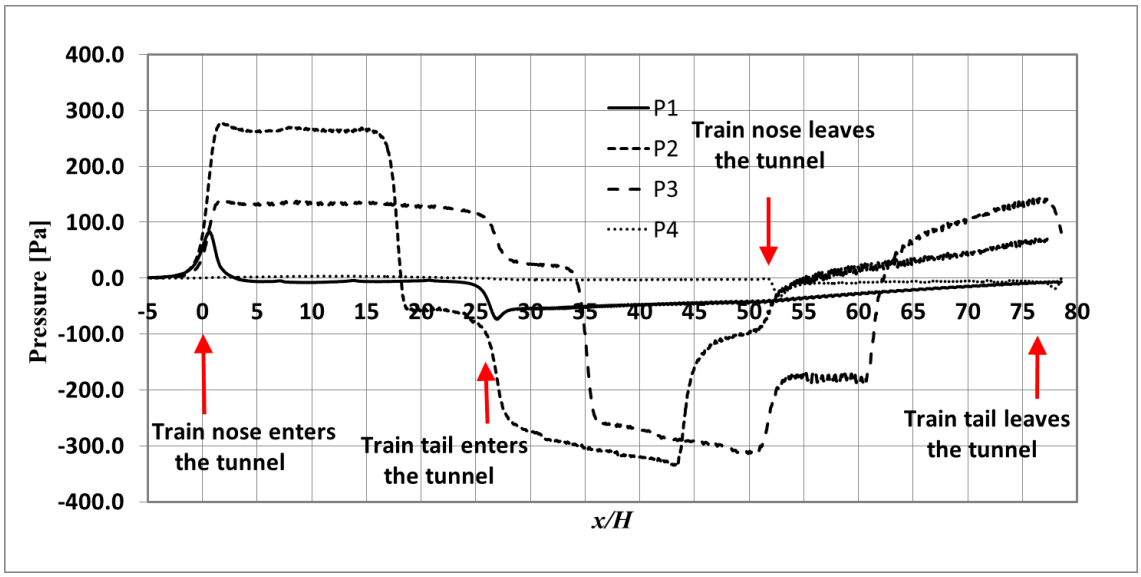

Figure 41 Short tunnel; Static pressure histories at the monitoring points.

Once the train enters the tunnel, there is a slight increase in the pressure at point P1. This increase in pressure is quickly disappears after the train nose and the pressure at point P1 is nearly the same as the environment except some variation when the enter-carriage gaps

passes the point. When the tail of the train enters the tunnel, there is a drop of the pressure at the entrance that is build-up regularly to zero when the tail of the train leaves the tunnel.

The largest pressure is calculated at point P2 as it reaches a maximum pressure once the train nose enters the tunnel and showed some small fluctuations before the train nose passes it. The passes of the train nose causes a drop of the pressure at point P2. This is followed by another drop in the pressure at the moment the tail of the train enters the tunnel. Along the length the train is passing the point there is a gradual decrease in the static pressure at point P2 until the tail passes the point after which there is a build-up of the pressure. There is also another increase of the pressure at point P2 when the train nose leaves the tunnel. The pressure at point P2 continues to increase until the tail of the train leaves the tunnel at which the pressure stabilized back to zero. Exactly similar trend to that at point P2 has been obtained at point P3. However, the maximum pressure at pint P3 ahead of the train is about half of that at point P2. Although the drop of the pressure at point P3 due to the passes of the train nose is of similar magnitude to that at point P2, the drop of pressure due to the entrance of train tail is about half of that at point P2. This makes the static pressure at point P3 while the train is passing the point is comparable to that at point P2. As point P3 is closer to the tunnel exit that P2, the increase of the static pressure at point P3 due to the train nose leaving the tunnel is about twice the increase in the pressure of point P2. However, the increase in the pressure of P3 due to the passes of the train tail is similar to that when the train tail passes point P2. This makes the static pressure at P3 when the train passes the point more than the pressure at point P2 when the train passes the point. Finally when the train tail exits the tunnel, the pressure at point P3 stabilized at zero. There is no significant effect of the train enters the tunnel at point P4 (tunnel exit). The only effect is when the train nose passes the point, at which there is a slight drop in the pressure which quickly build-up to zero when the train is completely exits the tunnel.

Figure 42, Figure 43, Figure 44 and Figure 45 show the time rate of change of pressure at point P1, P2, P3 and P4, respectively. It can be seen that the large pressure gradients at the four points occur at specific incidences such as when the train nose enters the tunnel,

when it passes the point, when the tail of the train enters the tunnel, when the tail of the train passes the point, when the nose of the train exits the tunnel and when the tail of the train exits the tunnel.

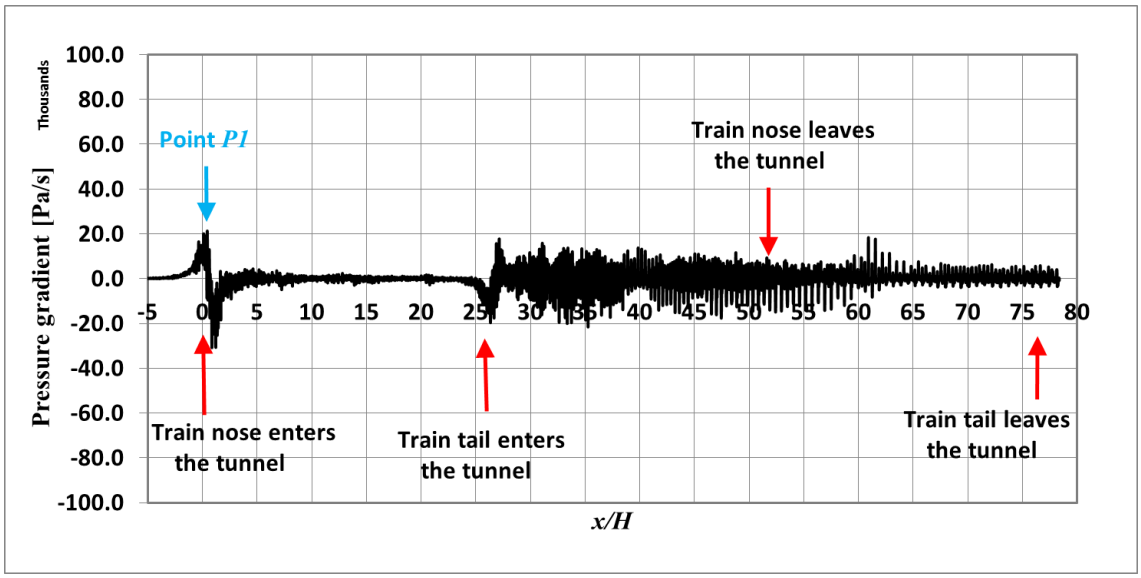

Figure 42 Short tunnel; Pressure gradient at point P1 shown in Figure 40.

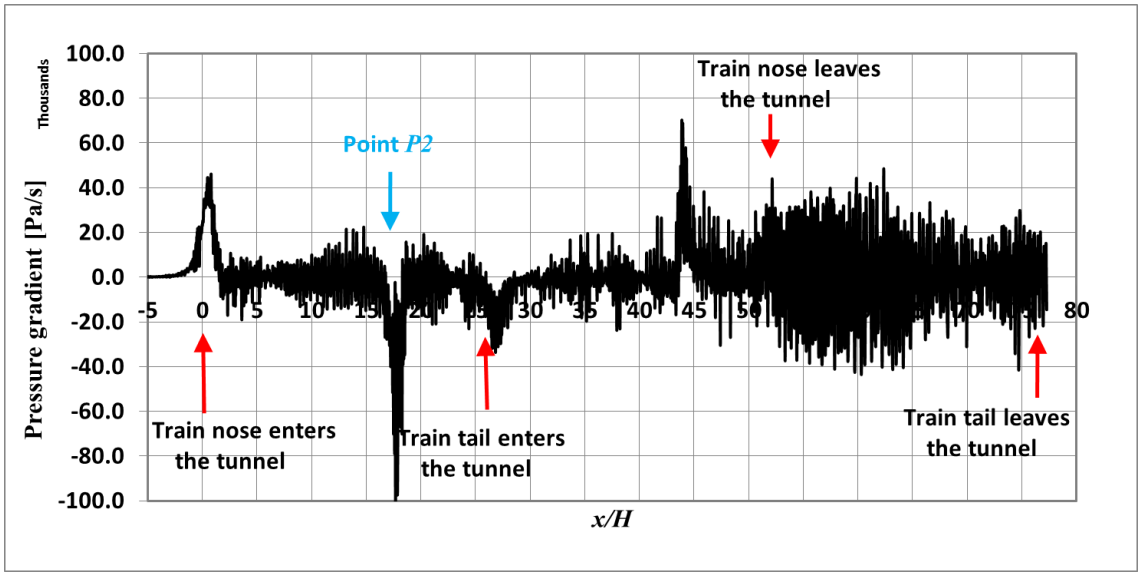

Figure 43 Short tunnel; Pressure gradient at point P2 shown in Figure 40.

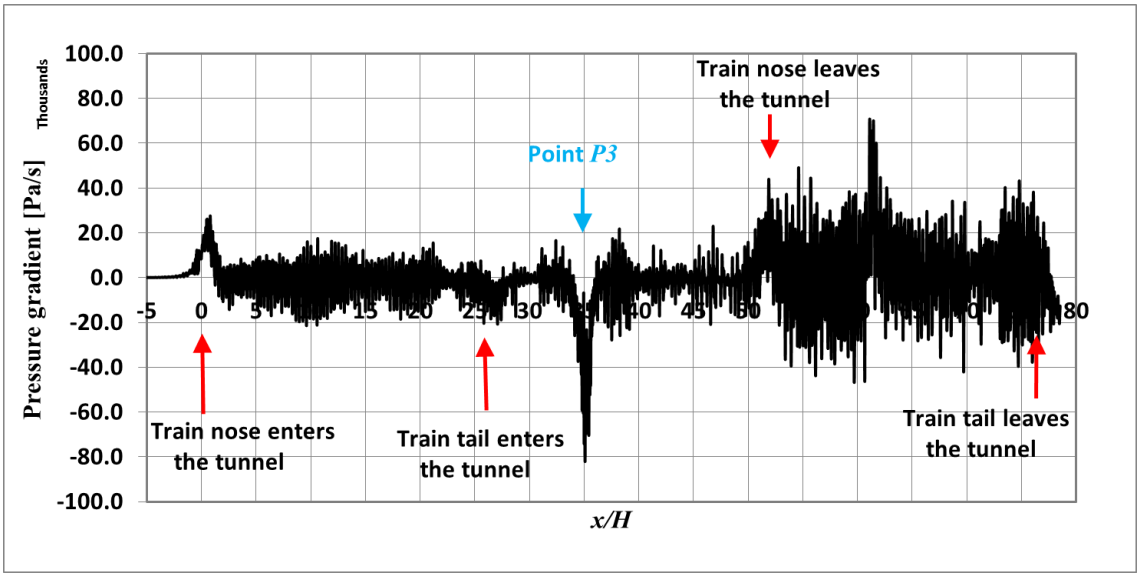

Figure 44 Short tunnel; Pressure gradient at point P3 shown in Figure 40.

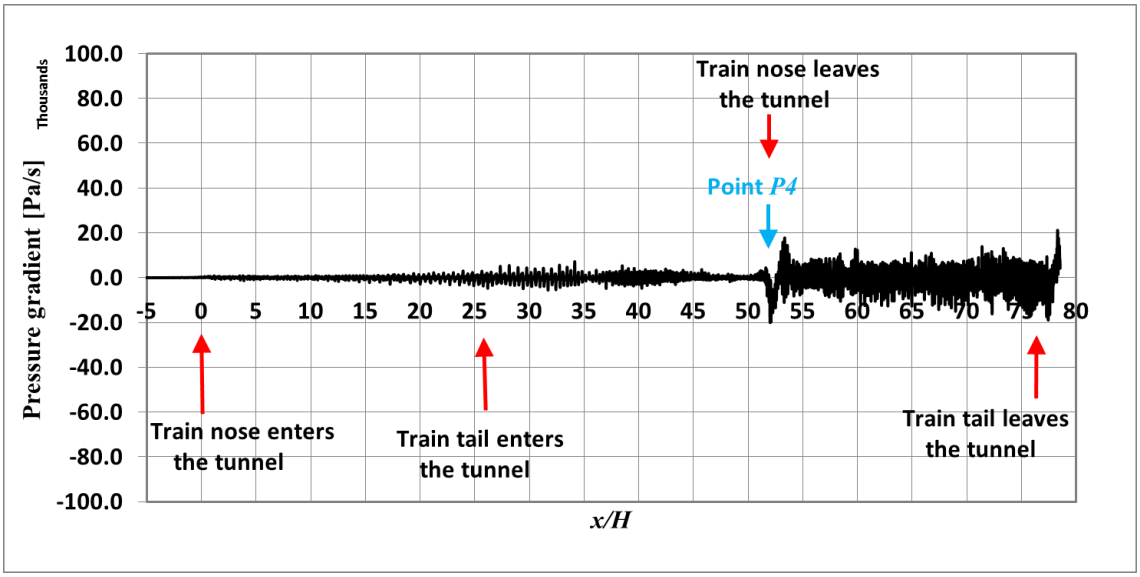

Figure 45 Short tunnel; Pressure gradient at point P4 shown in Figure 40.

There are also some small variations in the pressure when the inter-carriage gaps pass the points but the effect is relatively small. It has been noticed that for all the points there is a large oscillations in the pressure gradient once the train tail passes the point. This is due to the highly turbulent nature of the wake that makes the pressure vary significantly. This variation in the wake pressure affects the pressure ahead of the train which is reflected as some variations in the pressure gradient before the train nose approaches the point. This can be seen clearly in the pressure gradients at point P2 and P3 and slightly at point P4.

6.3 ICE2 train passing a long tunnel

In this section the results from the CFD simulation of the ICE2 passing through the long tunnel (double the length of the previous tunnel) are presented. In the first part, the velocity in the tunnel is described in terms of the velocity history at different points along the tunnel length. Velocity profiles are also presented at different sections ahead of the train and in the wake flow and planes coloured with velocity magnitude. In the second part, the static pressure inside the tunnel will be investigated using some monitoring points along the tunnel length.

6.3.1 Velocity distribution in the tunnel

Figure 46 shows the normalised velocity magnitude at the three monitoring pints C1, C2 and C3. The distance between the three points and the tunnel entrance are the same those shown in Figure 22. Before the train reaches the points, the same velocity magnitudes are observed. When the nose of the train passes the points, a drop in velocity is observed followed by a sudden increase. Along the length of the first car, there is no significant difference in the velocities at the three points. There is a large difference between the velocity at C1 and those at C2 and C3. To explain this, the longitudinal velocity component at the three points is plotted in Figure 47.

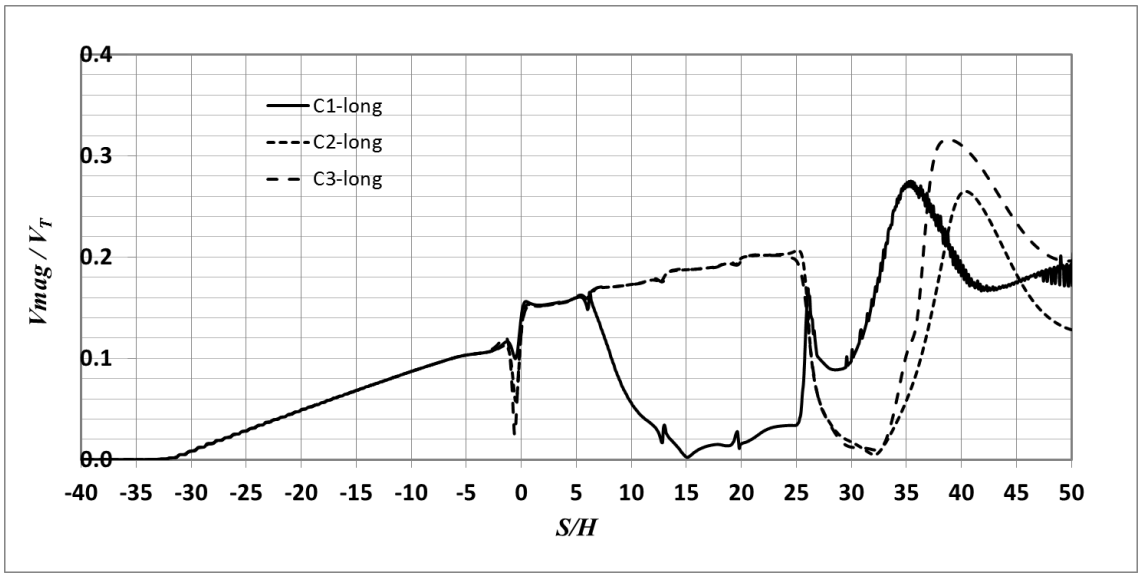

Figure 46 Long tunnel; Velocity magnitude at points C1, C2 and C3 shown in Figure 22.

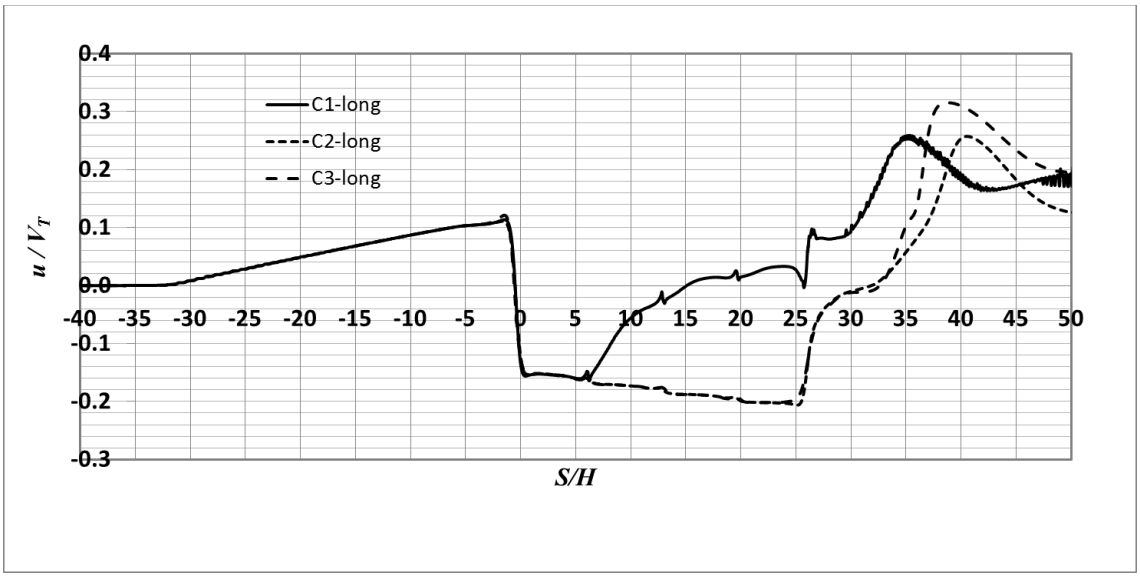

Figure 47 Long tunnel; Velocity component in the direction of train travel at points C1, C2 and C3 shown in Figure 22

It can be seen from Figure 47 that the three points have negative velocity components along the first car. After the first car, the longitudinal velocity at points C2 and C3 remains negative along the length of the train while the velocity at C1 changes to be positive after the first car.

Figure 48 shows the symmetry plane coloured by the velocity magnitude and Figure 49 shows the same plane coloured by the longitudinal velocity component. The slipstream is observed as a small belt of air around the train which moves in the direction of train travel. The thickness of the slipstream is shown to increase along train length. Due to point C1 being the closest point to the train it experiences some reversed flow along the first car. After the first car, the slipstream is thicker and thus point C1 is immersed in it and the surface of the train and thus the velocity component is positive. This is further explained in Figure 50 in which velocity vectors are drawn at the symmetry plane.

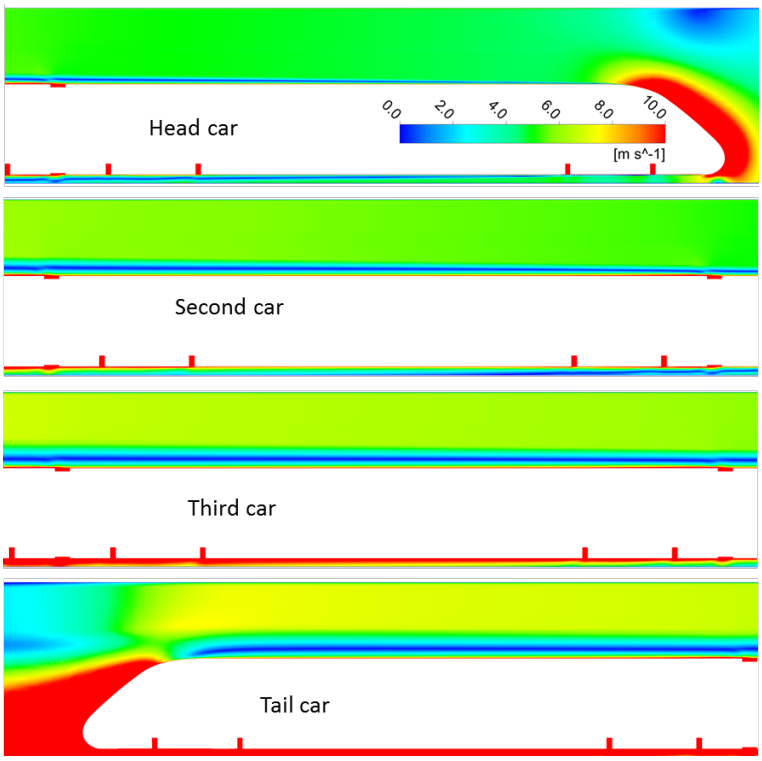

Figure 48 Long tunnel; Symmetry plane coloured by the velocity magnitude, showing the flow around the train in the tunnel.

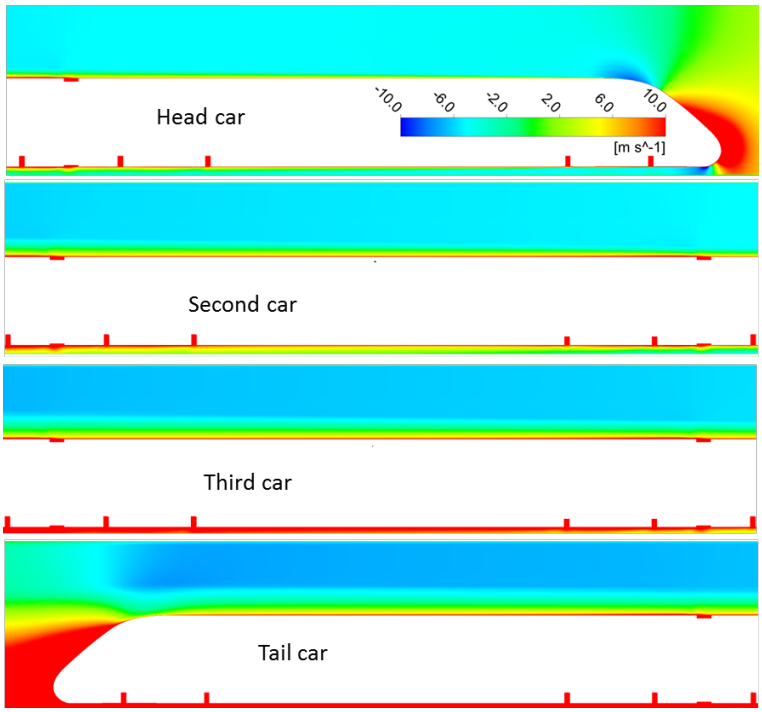

Figure 49 Long tunnel; Symmetry plane coloured by the velocity component in the direction of train travel, showing the flow around the train in the tunnel.

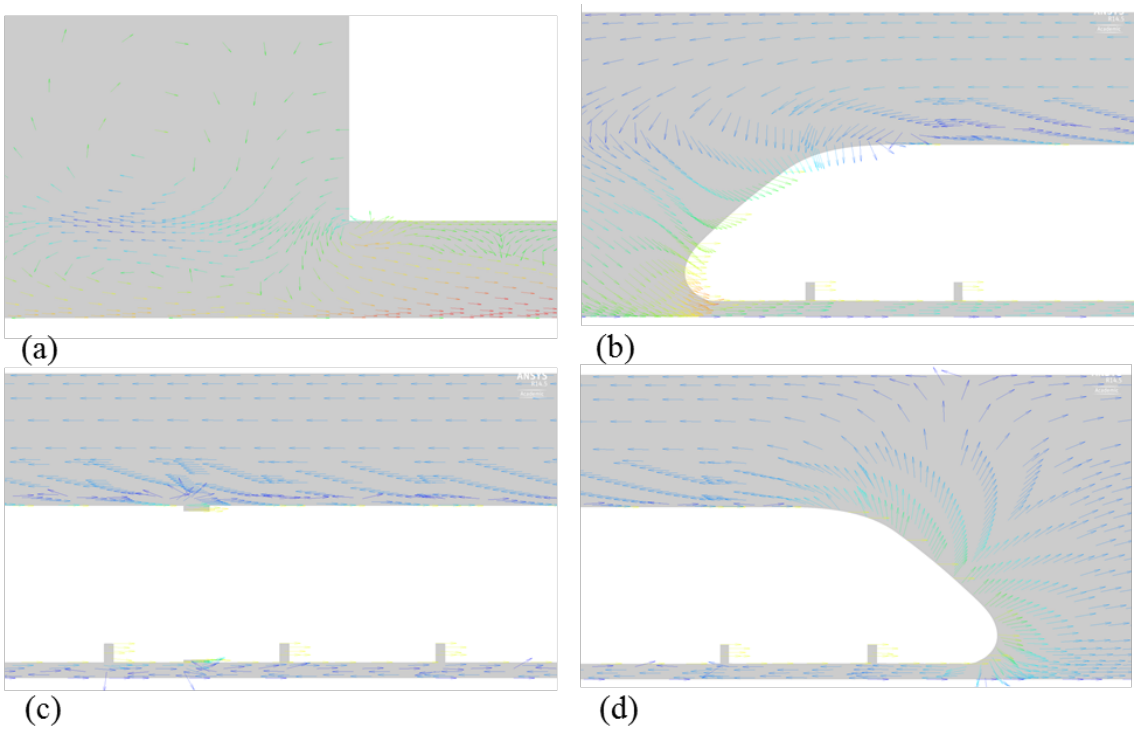

Figure 50 Long tunnel; Velocity vectors at the symmetry plane, showing the flow around the train in the tunnel.

Figure 51 shows the symmetry plane coloured by the longitudinal velocity component. The figure shows that the air is moving in the direction of train travel ahead of the train. In the wake flow, the air in the lower half of the tunnel moves in the direction of the train while in the upper half some of the air moves in the opposite direction. Along the length of the train, the air moves backward except in the slipstream region.

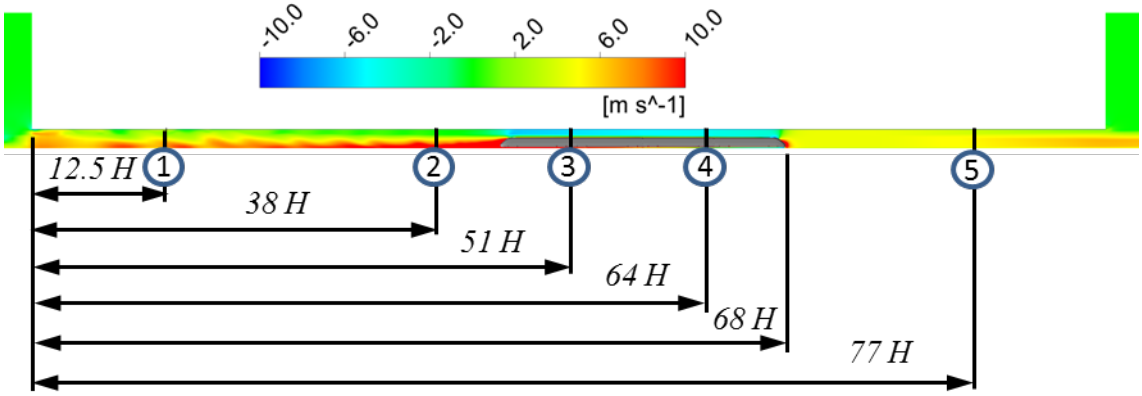

Figure 51 Long tunnel; Symmetry plane coloured by the velocity component in the direction of train travel, showing the distance of five sections from the tunnel entrance.

Figure 52 shows longitudinal velocity profiles at the five sections shown in Figure 51. It can be seen that the air around the train at sections 3 and 4 has negative velocity components except the small slipstream region. Also the slipstream thickness at section 3 (last car) is larger than that at section 4 (first car).

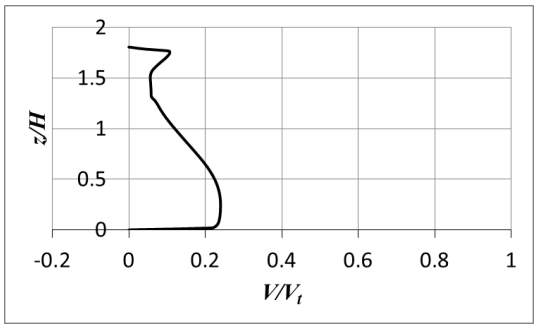

Section 1

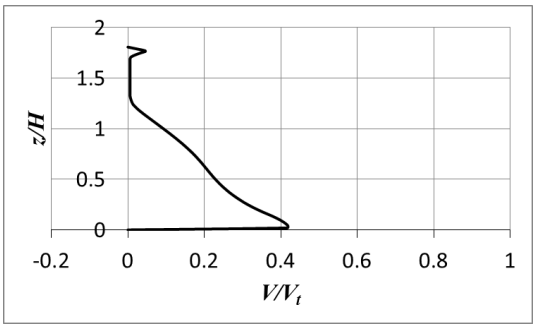

Section 2

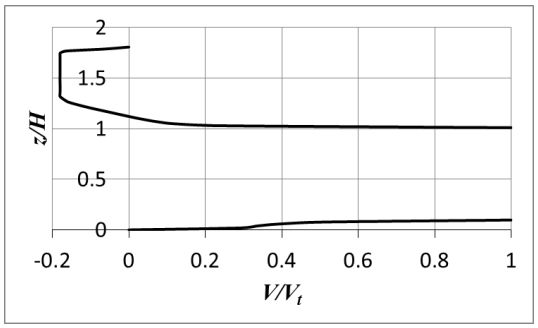

Section 3

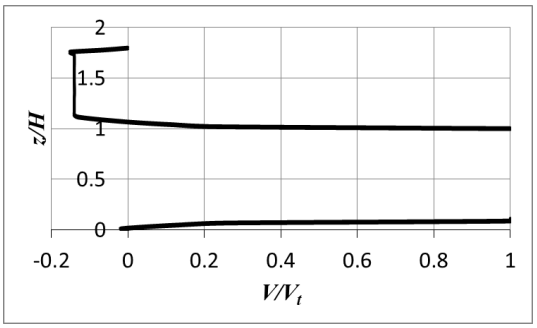

Section 4

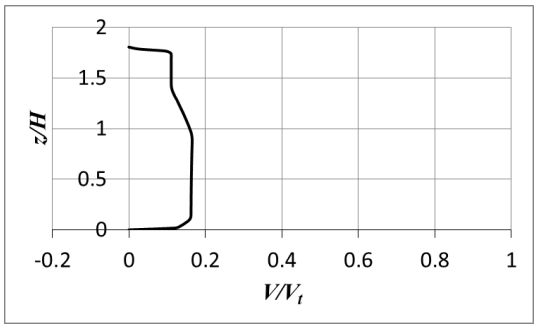

Section 5

Figure 52 Profiles of the velocity component in the direction of travel at the sections shown in Figure 51.

Figure 53 shows the vortical structure behind the train visualized by the iso-surface of the second invariant of the velocity gradient tensor. There is a large circulation at the tunnel portal due to the suction of air from the environment into the tunnel. The centre of this

vortex is shown clearly in Figure 54 using streamlines projected into the symmetry plane. There are also two symmetrical trailing vortices behind the train shown in Figure 53. The tunnel in Figure 53 is coloured by the static pressure showing the change of pressure ahead of the train, along the train and behind the train.

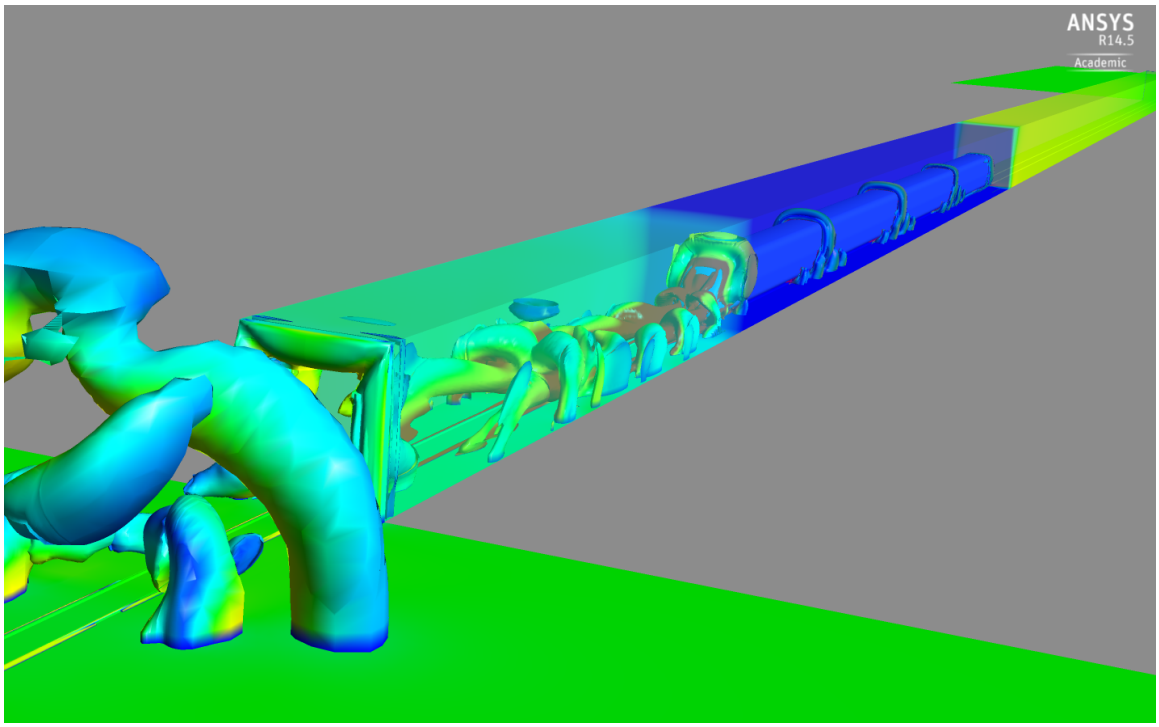

Figure 53 Short tunnel; Second invariant of the velocity gradient showing the large vortex at the tunnel entrance and the trailing vortices behind the train.

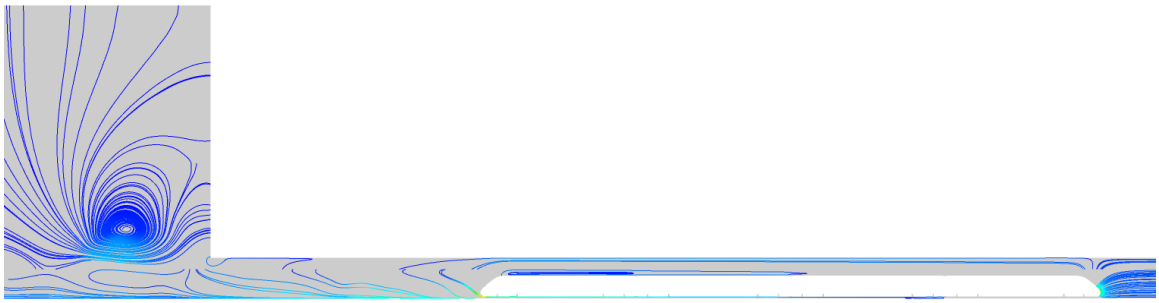

Figure 54 Long tunnel; streamlines projected on the symmetry plane.

6.3.2 Pressure distribution in the long tunnel

Figure 55 shows the pressure variation inside the tunnel as the train passes by means of colouring the symmetry plane with the static pressure. The maximum pressure occurs when the nose of the train enters the tunnel. The high pressure continues ahead of the train but shows a slight decrease once the tail of the train enters the tunnel. Furthermore, the static pressure at any point in the second half of the tunnel decreases as the train approaches the point.

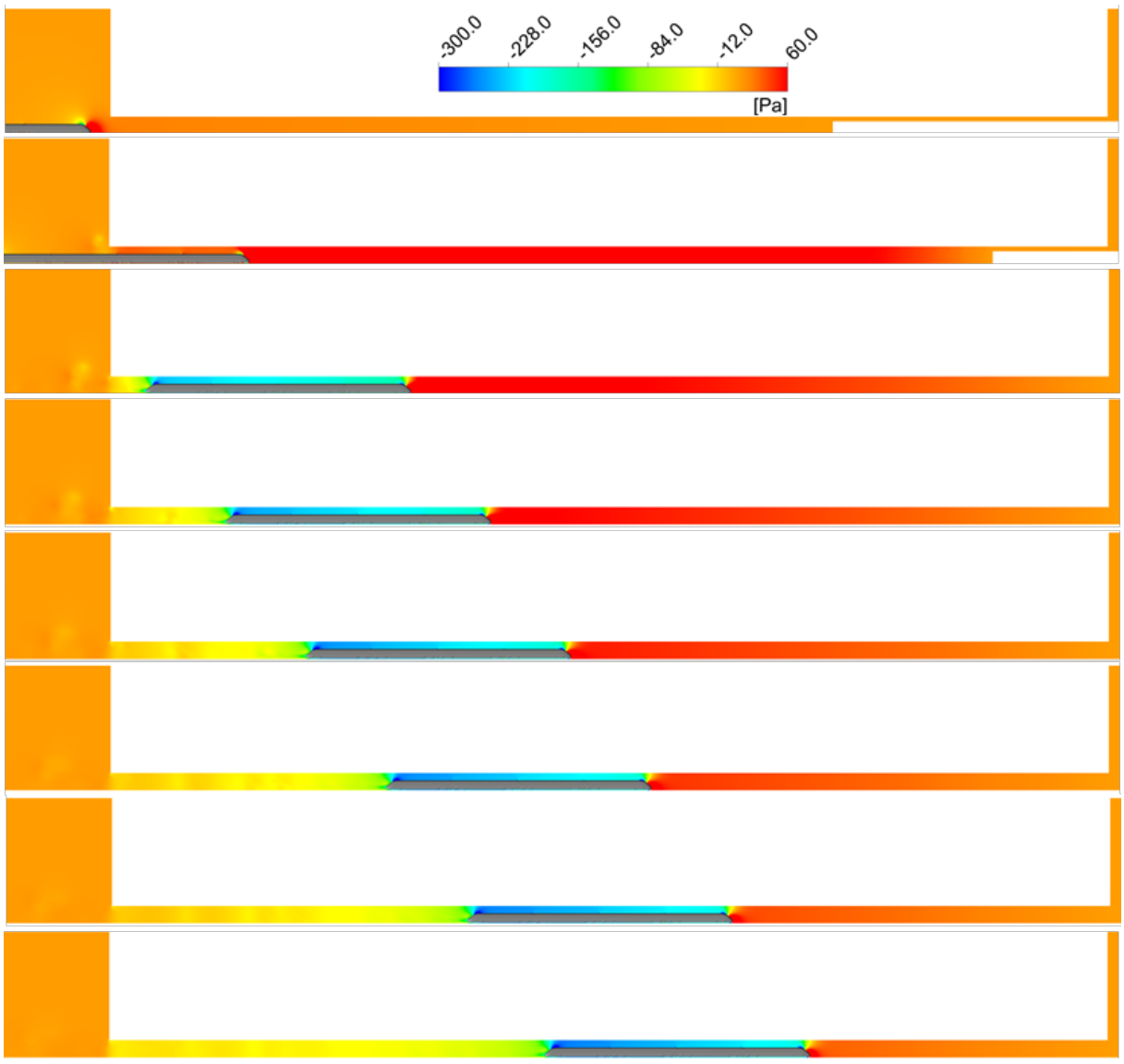

Figure 55 Symmetry plane coloured by static pressure showing the variation of the pressure inside the tunnel with the location of the train.

The time histories of the pressure at the four points shown in Figure 56, are exhibited in Figure 57.

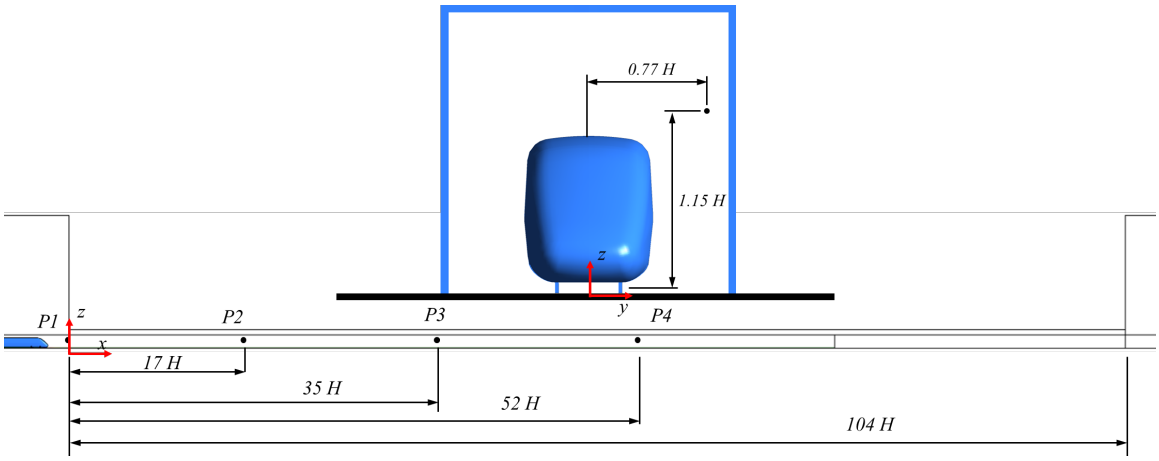

Figure 56 Long tunnel; Schematic diagram showing the monitoring points for the static pressure.

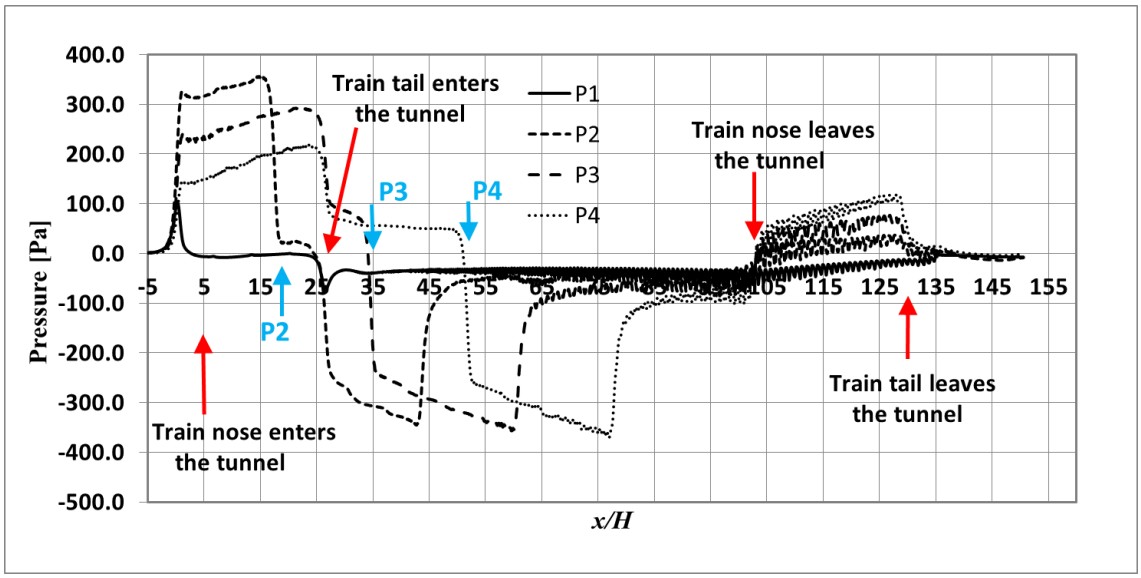

Figure 57 Long tunnel; Static pressure histories at the monitoring points shown in Figure 56.

When the nose of the train approaches the tunnel, there is a sudden increase in the tunnel pressure. This is reflected as an increase in the static pressure at point P1. Once the train enters the tunnel, the pressure at point P1 reduces towards ambient pressure except for small pressure fluctuations when the inter-carriage gaps pass that point. A decrease in static pressure is observed at point P1 when the tail of the train passes, which is due to the low pressure in the wake flow. The pressure at point P1 approaches zero once the tail of the train leaves the tunnel.

The maximum pressure occurs at point P2 when the train nose enters the tunnel. There are two occasions when a negative pressure transient occurs at P2. The first is when the nose of the train passes the section of the point. The second is when the tail of the train enters the tunnel. Along the train length, a gradual decrease in the pressure occurs until it reaches the maximum negative value when the tail of the train passes the point. After the train tail passes the point, the pressure rapidly increases while maintaining a negative value in the wake flow. When the train nose leaves the tunnel, the point pressure is positive until it eventually becomes zero when the whole train leaves the tunnel. Points P3 and P4 show the same pressure trend as P2 but with a lower pressure ahead of the train than was observed for point P2.

The distance between points P3 and P2 is the same as the distance between points P4 and P3. It can be seen from Figure 57 that the pressure drop between points P3 and P2 ahead of the train is the same as that between points P4 and P3. This means that the pressure drop is constant along the tunnel length. Also the pressure decreases at each point due to the passing of the train nose and due to the entrance of the tail to the tunnel. In addition, the increases in pressure due to the passing of train tail and due to the exit of the train nose out of the tunnel are also constant. Due to this effect the pressure at all the points is positive while the train is leaving the tunnel and the pressure gradient is positive inside the tunnel when the train is leaving. The pressure in the tunnel returns to zero when the train has fully left the tunnel.

Figure 58, Figure 59, Figure 60 and Figure 61 show the rate of change of pressure at points P1, P2, P3 and P4, respectively for the long tunnel. It can be seen that the large pressure gradient at the four points occurs at specific incidences which are when the nose of the train enters the tunnel, when the nose of the train passes the point, when the tail of the train enters the tunnel, when the tail of the train passes the point, when the nose of the train exits the tunnel and when the tail of the train exits the tunnel.

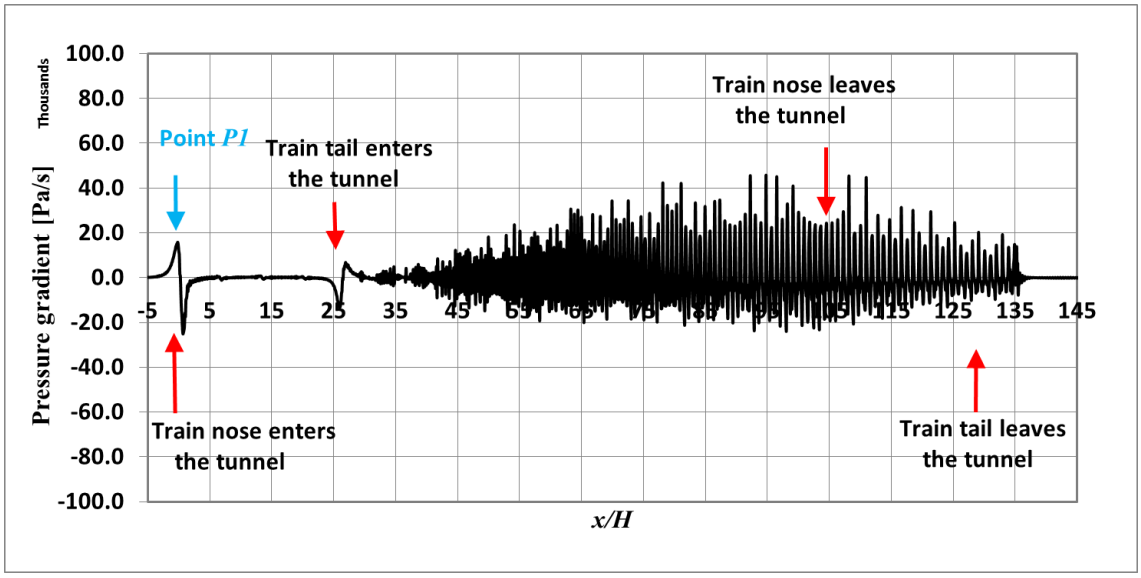

Figure 58 Long tunnel; Pressure gradient history at the monitoring point P1 shown in Figure 56.

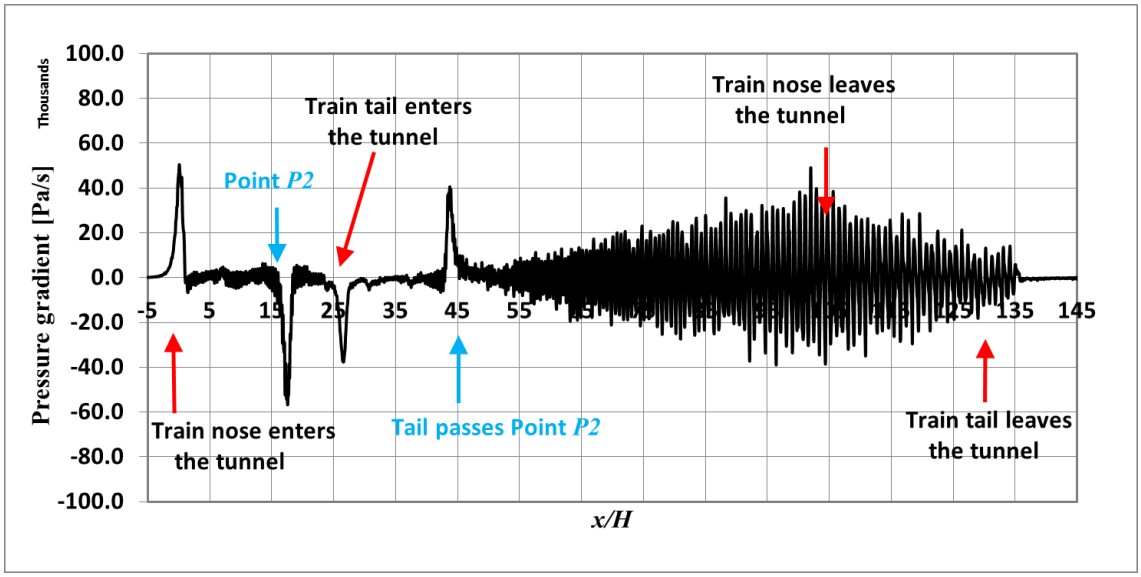

Figure 59 Long tunnel; Pressure gradient history at the monitoring point P2 shown in Figure 56.

Some small variations in pressure are observed when the inter-carriage gaps pass the points however this effect is relatively small. It has been noticed that for all the points there are large oscillations in the pressure gradient once the train tail passes the point. This is due to the nature of the highly turbulent flow in the wake that makes the pressure vary significantly. The variation in the wake pressure affects the pressure ahead of the train which is reflected in the form of variations in the pressure gradient before the train

nose approaches the point. This can be seen clearly in the pressure gradients at points P2 and P3 and to a lesser degree at point P4.

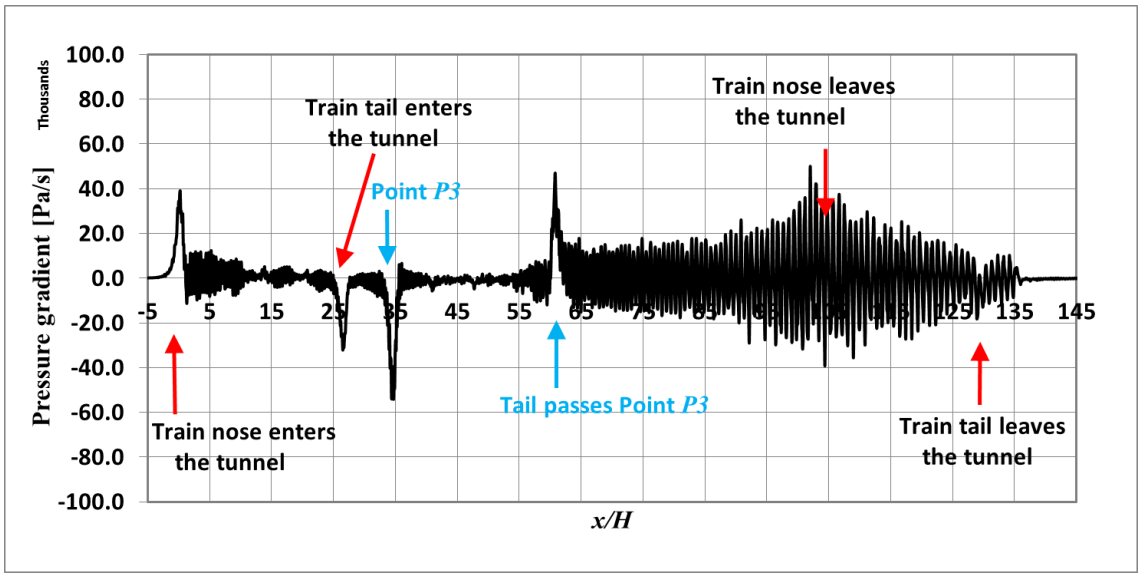

Figure 60 Long tunnel; Pressure gradient history at the monitoring point P3 shown in Figure 56.

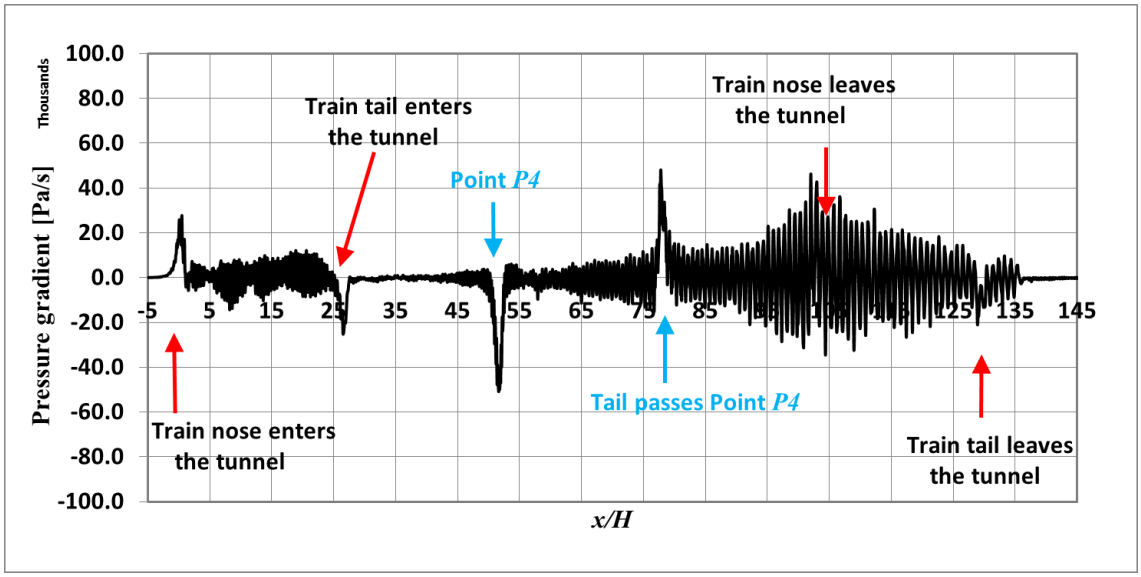

Figure 61 Long tunnel; Pressure gradient history at the monitoring point P4 shown in Figure 56.

Chapter 7. Discussion

Computational fluid dynamics (CFD) was used to simulate a 1/25th scale model train passing through tunnels. The results were validated against data from the European project "AEROTrain" (Sima et al., 2011) and Gilbert et al. (2013). The results were in a good agreement suggesting that the simulations were an accurate representation of the physical scenario.

In order to investigate the effect of tunnel length on the velocity and pressure fields around the train and inside the tunnel, two tunnel lengths were used: one twice the length of the other.

Figure 41 and Figure 57 show the static pressures inside the tunnel at the same points with the same distance from the tunnel portal for the short and long tunnels, respectively. Comparing the two figures shows that the length of the tunnel has a significant effect on the magnitude of the static pressure. For point P1, the maximum pressure is approximately 275 Pa for the short tunnel and 350 Pa for the long tunnel with about 75 Pa difference, which is about 27% increase. This difference in pressure is also similar for points P2, P3 and P4.

In both short and long cases, the effect of the train entrance into the tunnel is characterised as a sudden increase of pressure in the tunnel. When the nose of the train approaches any point, there is a generally a sudden decrease in the pressure. The pressure is almost constant along the length of the train. There is a reduction of the tunnel pressure when the tail of the train enters the tunnel and after tail passes, there is an increase in the static pressure. The tunnel pressure increases when the nose of the train leaves the tunnel and when the tail of the train leaves the tunnel, the pressure returns to atmospheric pressure.

The sudden increase and decrease in static pressure due to the entrance and exit of the train in to and out of the tunnel causes a pressure gradient along the tunnel length. Taking point P2 as an example, Figure 43 shows that the pressure gradient for the short tunnel is about 40,000 Pa/s when the nose of the train enters the tunnel and about 100,000 when the nose of the train passes that point. Figure 59 shows that, similar to the short tunnel, the pressure gradient is about 40,000 Pa/s when the train enters the tunnel and about

60,000 Pa/s when the nose of the train passes the measurement point. This indicates that the tunnel length has a significant effect on the pressure gradient and the magnitude of the static pressure.

In terms of the flow field inside the tunnel, the short and long tunnel simulations show that the flow moves ahead of the train in the direction of train travel. As the pressure ahead of the train is much larger than in the wake, the air in the confined space between the train and the tunnel moves backward. Figure 27 shows that the maximum velocity ahead of the train is when the train nose approaches the point with a normalised velocity of 0.19. Along the length of the train, the air moves backwards with a normalised velocity of approximately 0.1. The maximum velocity is found in the wake of the train with about 30% of the train speed.

The air flow above the train is different to the flow ahead of the train, where the maximum velocity was found. After the train nose passes the point a decrease in the velocity is observed in the wake flow.

For the long tunnel, Figure 47 shows same trend as the short tunnel in which the air flow increases when the train's nose approached the point the maximum normalised velocity of 0.12 occurs. After this a reverse flow velocity of 0.2 of the train speed occurs along the train length. The maximum slipstream velocity is found in the wake with a normalised value of 0.3.

It is observed that when comparing the air velocities from the short and long tunnels the increase in the static pressure in the long tunnel has a significant effect on the air velocity ahead of and along the train length. The high pressure ahead of the train increases the velocity of the reversed flow more in the case of the long tunnel than that of the short tunnel.

The simulations of the short and long tunnels show that there are two large vortices, one before the entrance of the tunnel and the other after the train leaves the tunnel. Inside the tunnel there are two trailing vortices behind the trains.

Chapter 8. Conclusions and Further work

Computational fluid dynamics using the sliding technique method have been used to investigate the pressure transit and flow in tunnels. In order to validate the method, a generic train similar the one used in the EU project AeroTRAIN has been placed in a virtual wind tunnel (the computation domain) and the obtained results deemed to be similar to those obtained in the AeroTRAIN project. After validating the sliding mesh technique, the method used to investigate the effect of tunnel length on the pressure transient. Simulations of a train moving through short and long tunnels were compared with experimental work and good agreement was obtained. A comparison between the data obtained from two mesh densities was conducted and good agreement between the results was observed. Based on the comparison between the simulations of the short and long tunnels, the following observations can be made:

- The pressure is the same for the same cross-sectional position in the tunnel.
- The air in the tunnel moves ahead of the train in the direction of the train movement.
- Due to the compressibility of the air, the velocity along the tunnel is not constant with an increase in the air velocity being observed when the train approaches a specific point in the tunnel.
- The maximum velocity and pressure in the tunnel occur when the nose of the train passes.
- Once the train passes a specific point in the tunnel there is a sudden reduction in the pressure and the air moves opposite to the direction of the train.
- Higher pressures are observed ahead of the train in the longer tunnel
- Lower velocities are observed ahead of the train in longer tunnels and the revered flow also has higher velocity.
- In general, there is a sudden increase in the pressure in the tunnel when the train enters and when the train nose leaves the tunnel.

- A sudden decrease in the tunnel pressure occurs when the tail of the train enters the tunnel and when the train nose passes.
- Once the train tail leaves the tunnel, the static pressure inside the tunnel quickly decreases towards atmospheric pressure.
- Although there is a large effect of the tunnel length on the static pressure in the tunnel, the pressure gradient is not affected significantly.
- Similar flow structures have been obtained in the wake flow in both the short and long tunnels.

The results in this thesis are based on the unsteady RANS using the SST *k-w* model. The mesh density is adequate for the RANS simulations. However, this method might not get the small instantaneous flow structures around the moving train that could affect the pressure variation. Thus it is recommended that a more accurate CFD technique such as Large Eddy Simulation can be used. Also the train underbody blockage has been simplified in this study to facilitate the mesh generation. It is also recommended that the simulations are repeated for a more detailed underbody blockage. This study is based on a single track tunnel. However, no attempt to investigate the effect of the tunnel length of a double track has been done.

Although, the long tunnel is double the length of the short tunnel another simulation might be required for an even longer tunnel to give a rigour conclusion.

References

Baker C., (2001), 'Flow and dispersion in ground vehicle wakes', *Journal of Fluids and Structures* 15, 7, 1031-1060, doi:10.1006/jfls.2001.0385.

Baker C., (2010a), The flow around high speed trains, Journal of Wind Engineering and Industrial Aerodynamics, 98, 6–7, 277–298, doi:10.1016/j.jweia.2009.11.002.

Baker C., (2010b), 'Train aerodynamic problems and solutions', Railway Strategies, April-May 2010, Available at: http://www.railwaystrategies.co.uk/article-page.php?contentid=10286&issueid=317.

Baker, C., (2014), 'A review of train aerodynamics, part 1—fundamentals' The Aeronautical Journal, vol 118, no. 1201.

Baker C., Dalley S J., Johnson T., Quinn A., and Wright N. G., (2001), 'The slipstream and wake of a high-speed train', *Proceedings of the Institution of Mechanical Engineers F Journal of Rail and Rapid Transit*, 215, 83-99, doi:10.1243/0954409011531422.

Baker C., Gilbert T., and Jordan S., (2013c), 'The validation of the use of moving model experiments for the measurement of train aerodynamic parameters in the open air', *Proceedings of the World Congress on Rail Research, Sydney, Australia.*

Baker, C., Hemida H., Iwnicki S., Xie G., and Ongaro D., (2011), "The integration of crosswind forces into train dynamic modelling" Journal of Rail and Rapid Transit Vol. 225, Issue 2, pp. 154-164.

Baker C., Jordan S J., Gilbert T., Sterling M., Quinn A., Johnson T., and Lane J., (2012a), 'Transient aerodynamic pressures and forces on trackside and overhead structures due to passing trains. Part 1 Model scale experiments', *Journal of Rail and Rapid Transit*, 228 36 – 69, 10.1177/0954409712464859.

Baker, C., Jordan S., Gilbert, T., Quinn A. Sterling, M., Johnson T., and Lane J., (2012b), 'Transient aerodynamic pressures and forces on trackside and overhead structures due to passing trains. Part 2: Standards applications' Journal of rail and rapid transit, Vol 228, no. 4, pp. 36-69.

Baker C., Quinn A., Sima M., Hoefener L., and Licciardello R., (2013a), 'Full-scale measurement and analysis of train slipstreams and wakes: Part 1 Ensemble averages', *Proceedings of the Institution of Mechanical Engineers, Part F: Journal of Rail and Rapid Transit*, doi:10.1177/*0954409713485944*.

Baker C., Quinn A., Sima M., Hoefener L., and Licciardello R., (2013b), 'Full-scale measurements and analysis of train slipstreams and wakes—Part 2', Journal of rail and rapid transit, vol. 228 no. 5 468-480.

Baker C., Sterling M., Bouferrouk A., O'Neil H., Wood S., and Crosbie E., (2008), 'Aerodynamic forces on multiple unit trains in cross winds', Proceedings of the Conference on Bluff Body Aerodynamics and its Applications, Milano, Italy.
CEN., (2003), Railway Applications – Aerodynamics Part 2 Aerodynamics on Open Track E BS EN 14067-2:2003.

CEN., (2009), Railway Applications – Aerodynamics Part 4 Requirements and test procedures for aerodynamics on open track, BS EN 14067-4:2005+A1:2009.

CEN., (2010), Railway Applications – Aerodynamics. Part 6 Aerodynamics Tests for crosswind assessment, BS EN 14067-6:2010.

Cheli F., Ripamonti F., Rocchi D., and Tomasini G., (2010), Aerodynamic behaviour investigation of the new EMUV250 train to cross wind. Journal of wind engineering and industrial aerodynamics Volumes 98 Pages 189-201.

Diedrichs B., (2003), 'On computational fluid dynamics modelling of crosswind effects for high-speed rolling stock', Proceedings of the Institution of Mechanical Engineers, Part F: Journal of Rail and Rapid Transit, 217: 203, 10.1243/095440903769012902.

Flynn D., Hemida H.. Soper D., and Baker C., (2014), 'Detached-eddy simulation of the slipstream of an operational freight train' Wind engineering and industrial aerodynamics, DOI: 10.1016/j.jweia.2014.06.016.

Gil N., Baker C., and Roberts C., (2008), "The Measurement of Train Slipstream Characteristics Using a Rotating Rail Rig", BBAA VI International Colloquium on Bluff Bodies Aerodynamics and Applications , Milan, Italy.

Gilbert T., Baker C., and Quinn A., (2013), "Gusts by high-speed trains in confined spaces and tunnel", Journal of wind engineering and industrial aerodynamics 121(2013) 39-48.

Golovanevskiy V A., Chmovzh V V., and Girka V Y., (2012), 'On the optimal model configuration for aerodynamic modelling of open cargo railway train', Journal of wind engineering and industrial aerodynamics Volumes 107-108 Pages 131-139.

Hemida H., and Baker, C., (2012). "The Calculation of Train Slipstreams using Large-Eddy Simulation" Journa of Rail and Rapid Transit, doi:10.1177/0954409712460982, 2012.

Hemida H., and Baker C., (2010). 'LES of the flow around a freight wagon subjected to crosswind', Computers & Fluids, Vol. 39, Issue 10, pp. 1944-1956.

Hemida H., Gil N., and Baker C., (2010), 'Large-Eddy Simulation of Train Slipstream'. J. Fluids Eng. Vol. 132, Issue 5, 051103, doi:10.1115/1.4001447, 2010.

Hemida H., and Krajnovic' S., (2009), 'LES Study of the Influence of Yaw Angles and Nose Shape on Flow Structures Around Trains'. Journal of Wind Engineering and Industrial Aerodynamics, doi:10.1016/j.jweia.2009.08.012, 2009.H, 2009.

Hemida H., and Krajnović S., (2010), 'LES study of the influence of the nose shape and yaw angles on flow structures around trains', *Journal of Wind Engineering and Industrial Aerodynamics*, 98, 1, 34-46 10.1016/j.jweia.2009.08.012.

Hong-qi T., (2009), 'Formation mechanism of the aerodynamic drag of high-speed train some reduction measures'. Springer.

Howe M. S., (2003a), 'On the infrasound generated when a train enters a tunnel'. Journal of Fluids and Structures 17 (2003) 629–642

Howe M. S., (2003b), 'Design of a tunnel-entrance hood with multiple windows and variable cross-section'. Journal of Fluids and Structures 17 (2003) 1111–1121

Howe M. S., Iida M., Fukuda T., and Maeda T., (2000), 'Theoritical and experimental investigation of the compression wave generated by a train entering a tunnel with a flared portal'. Journal of fluid mechanics, vol. 425, pp. 111–132.

Howe M. S., Iida M., Fukuda T., and Maeda T., (2003), 'Influence of an unvented tunnel entrance hood on the compression wave generated by a high-speed train'. Journal of fluids and structures 17 (2003) 833-853

Huang S., Hemida H., and Yang M., (2014). 'Numerical Calculations of the Slipstream of the CRH2 High-speed Train', Journal of Rail and Rapid Transit, DOI: 10.1177/0954409714528891.

Jönsson M., Haff J., Richard H., Loose S., and Orellano A., (2009), 'PIV Investigation of the flow field underneath a generic high speed train configuration', Euromech 509, External aerodynamics of railway vehicles, trucks, buses and cars, Berlin, Germany.

Khayrullina A., Blocken B., Janssen W., and Straathof J., (2014), 'CFD study on aerodynamic of a train passing an underground railroad platform'. Eindhoven university of technology.

Ko Y., Chen C., Hoe I., and Wang S., (2012), 'Field measurement of aerodynamic pressures in tunnels induced by high speed trains'. *Journal of wind engineering and industrial aerodynamics*. Vol. 100, issue 1, pp. 19-29.

Krylove V., (2001), 'Noise and vibrations from high-speed train'. Thomas Telford publishing, Thomas Telford Ltd. First published 2001.

Liu Y., Hemida, H., and Liu Z., (2013), 'Large Eddy Simulation of the flow around a train passing a stationary freight', Journal of Rail and Rapid Transit, DOI: 10.1177/0954409713488096, 2013.

Quinn A., Hayward M., Baker C., Schmid F., Priest J., and Powrie W., (2010), 'A full-scale experimental and modelling study of ballast flight under high-speed trains, Proceedings of the Institution of Mechanical Engineers', Part F: Journal of Rail and Rapid Transit 224, 2 61-74, 10.1243/09544097JRRT294.

Reiterer M., Ehrendorfer K., and Sockel H., (2002), 'Experimental Investigation of the Micro Pressure Wave' *Notes on Numerical Fluid Mechanics and Multidisciplinary Design*, Vol 79, pp 290-301.

Ricco P., Baron A., and Molteni P., (2007), 'Nature of pressure waves induced by a high-speed train travelling through tunnel', Journal of wind engineering and industrial aerodynamics, vol. 95 (8), pp. 781-808.

Sima M., Grappein E., Weise M., Paradot N., Hieke M., Baker C., Licciardello R., Couturier M., (2011),. 'Presentation of the EU FP7 AeroTRAIN project and first results', 9th world congress on railway research May 22-26.

Sterling M., Baker C., Jordan S., and Johnson T., (2008), 'A study of the slipstreams of high speed passenger trains and freight trains', Proceedings of the Institute of Mechanical Engineers Part F: Journal of Rail and Rapid Transport. Vol. 222, 177-19, 10.1243/09544097JRRT133.

Suzuki M., Ido A., Sakuma Y., and Kajiyama H., (2008), 'Full-scale measurement and numerical simulation of flow around high-speed train in tunnel'. Journal of mechanical systems for transportation and logistics, Volume 1 number 3.

Vardy A.E., (2008), 'Generation and alleviation of sonic booms from rail tunnels' Proc. ICE s' ProComput. Mech., 161 (3) (2008). pp. 107–119.

Wilcox D. C., (1994), 'Simulation of transition with a two-equation turbulence model', AIAA journal, Volume 32, No 2, February 1994.